

AMES
GRANT
IN-25-CR
319236
P. 79

FRICTION AND WEAR OF TPS FIBERS

A STUDY OF THE ADHESION AND FRICTION OF HIGH MODULUS FIBERS

NAG-2-444

FINAL REPORT

TO

NATIONAL AERONAUTICS AND SPACE ADMINISTRATION
AMES RESEARCH CENTER
MOFFETT FIELD, CA 94035

FROM

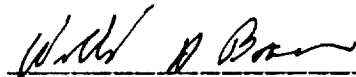
Willard D. Bascom

and

Ilzoo Lee

Materials Science and Engineering Department
University of Utah, Salt Lake City, UT 84112

November 1990



W. D. Bascom
Principal Investigator

(NASA-CR-187666) FRICTION AND WEAR OF TPS
FIBERS: A STUDY OF THE ADHESION AND FRICTION
OF HIGH MODULUS FIBERS Final Report (Utah
Univ.) 79 p

CSCL 07D

N91-13515

Unclass

G3/25 0319236

TABLE OF CONTENTS

TABLE OF CONTENTS	2
INTRODUCTION	3
PART I FRICTION AND ADHESION OF SILICA FIBERS IN AIR AND LIQUID ENVIRONMENTS.....	4
BACKGROUND.....	4
THEORY OF CONTACT ADHESION AND FRICTION.....	4
Contact Adhesion.....	5
Friction.....	8
MATERIALS AND EXPERIMENTAL PROCEDURES.....	10
Materials.....	10
Adhesion Measurements.....	12
Friction Measurements.....	15
Adhesion and Friction Measurements in Liquids.....	18
Contact Angle Measurements.....	18
DATA ANALYSIS.....	19
RESULTS AND DISCUSSION	28
Adhesion and Friction of Dry Fibers in Air.....	28
Friction Measurement in Liquids.....	35
CONCLUSIONS	40
PART II FRICTION AND ADHESION OF SILICA FIBERS COATED WITH ADSORBED ORGANIC MONOLAYERS	42
BACKGROUND.....	42
MATERIALS AND FILM PERPARATION	42
Materials	42
RESULTS AND DISCUSSION	44
Wettability, Friction and Shear Strength of Octadecylamine Coated Fibers.....	44
Wettability, Friction and Shear Strength of Alkyl Silanes.....	51
CONCLUSIONS	55
PART III ADHESION AND FRICTION OF POLYMER FILMS COATED ON SILICA FIBERS	56
BACKGROUND.....	56
EXPERIMENTAL MATERIALS AND METHODS	56
RESULTS AND DISCUSSION	57
CONCLUSIONS	64
PART IV FRICTIONAL BEHAVIOR OF TPS FIBERS	65
BACKGROUND.....	65
EXPERIMENTAL.....	65
RESULTS.....	65
CONCLUSIONS	73

INTRODUCTION

The adhesional and frictional forces between filaments in a woven fabric or felt strongly influence the processability of the fiber and the mechanical durability of the final product. Even though the contact loads between fibers are low, the area of contact is extremely small giving rise to very high stresses; principally shear stresses. One consequence of these strong adhesional and frictional forces is the resistance of fibers to slide past each other during weaving or when processed into nonwoven mats or felts. Furthermore, the interfiber frictional forces may cause surface damage and thereby reduce the fiber strength. Once formed into fabrics, flexural handling and manipulation of the material again causes individual filaments to rub against each other resulting in further surface damage. This problem is especially pertinent to high modulus, brittle fibers such as those used in thermal protection systems (TPS).

The adhesion and friction of organic fibers, notably polyethylene terephthalate (PET) fibers, have been extensively studied notably by Briscoe and coworkers (1-5). There has been very little work reported on high modulus inorganic fibers with the notable exception of work by Roselman and Tabor (6) on carbon fibers.

In the work reported here an extensive study was made of the adhesion and friction of flame drawn silica fibers in order to develop experimental techniques and a scientific basis for data interpretation. Subsequently, these methods were applied to fibers of interest in TPS materials.

PART I: FRICTION AND ADHESION OF SILICA FIBERS IN AIR AND LIQUID ENVIRONMENTS

BACKGROUND

Contact adhesion and sliding friction are important to understanding solid-solid interactions. They provide insight into the molecular forces of attraction and the mechanical properties of solid surfaces. Our current understanding of friction derives primarily from the work of Bowden and Tabor (7,8). They emphasize that the force of attraction between two surfaces has two components, weak, long-range van der Waal's interaction which can act over a significant fraction of the nominal area of contact and potentially much stronger short-range interactions, which may be ionic, covalent or metallic, depending on the chemistry of the surfaces involved. These stronger forces have a much shorter range of interaction, about one atomic diameter, and are generally repulsive resulting in an equilibrium distance of approach between two similar solids of z_0 which is of the order of one atomic diameter, i.e. 0.2nm.

In the interpretation of friction data, it is rarely possible to know the actual area of contact. Most solid surfaces, even when carefully prepared have some degree of surface roughness and so the contact is between the high points of the roughness, i.e. the surface asperities. However, this problem of knowing the true contact area is avoided in the work reported here by measuring the friction between smooth, small diameter filaments.

In the present study, flame drawn silica fibers were used which when examined using scanning electron microscopy (SEM) appear to be smooth and circular in cross-section at a magnification of 12,000X. Consequently, it is reasonable to assume the nominal area of contact and the actual area of contact are equal. Moreover, the circular cross-section allows the calculation of the contact area from Hertzian elastic deformation and the contact adhesion and surface strength from elementary theories of solid/solid interactions.

THEORY OF CONTACT ADHESION AND FRICTION

Contact Adhesion: Adhesion is the result of attractive forces between two surfaces in close contact and may be the result of ionic, covalent, metallic, hydrogen bonding or van der Waals' forces. The adhesion between non-metallic solids is primarily the result of weak van der Waals' forces which are effective over a distance of less than 10 nm (9). Assuming the elementary theory of the forces of attraction and repulsion between atoms or molecules on the two interacting surfaces we assign a value of the equilibrium separation, z_0 , at which the net resulting force just vanishes in the absence of an external force. The interaction energy at equilibrium attains its minimum value as shown in Figure 1.

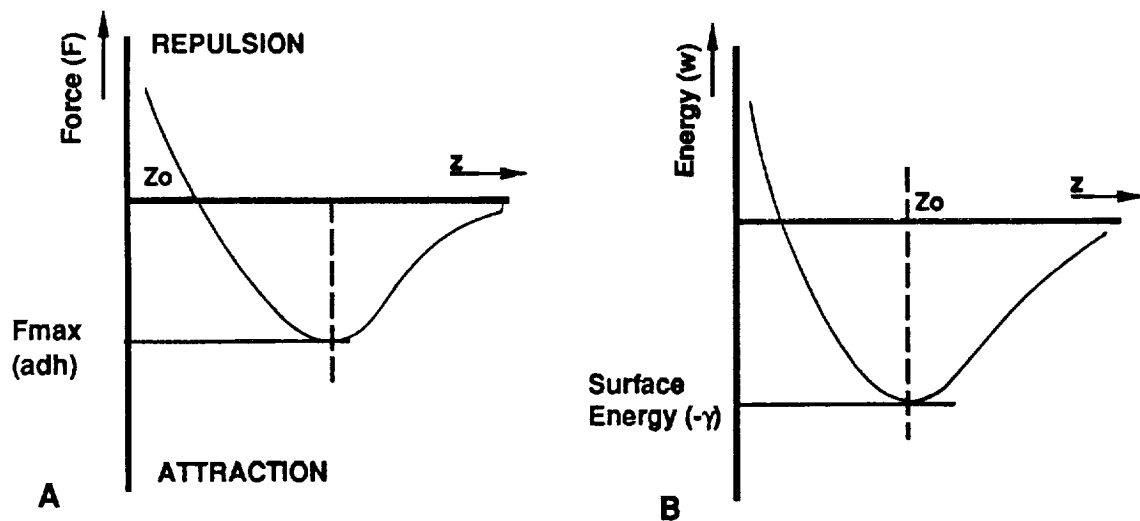


Figure 1 - Interactive force (A) and energy (B) between two solids as a function of separation distance (z).

For separations large compared with the equilibrium distance, z_0 , but still within the nonretarded region^a, the attractive force between two crossed cylinders having equal radii (R) is,

$$F = - \frac{A_{12}R}{6z^2} \quad [1]$$

where z is the separation distance and A_{12} is the appropriate Hamaker constant. If the cylinders come into atomic contact, z

^a It is assumed that the Hamaker constant does not change with distance of separation.

reaches the equilibrium separation distance, z_0 . The attractive force and hence the force required to pull the surfaces apart is then,

$$F_0 = \frac{A_{12}R}{6z_0^2} \quad [2]$$

We assume here that the short-range repulsive forces do not appreciably affect the value of F_0 .

Consider now the force per unit area between two half plates which at small separations z is,

$$f = \frac{A_{12}}{6\pi z^3} \quad [3]$$

The maximum work of separation can be obtained in terms of the surface and interfacial energies,

$$\int_{\infty}^{z_0} f dz = (\gamma_1 + \gamma_2 - \gamma_{12}) = \frac{A_{12}}{12\pi z_0^2} \quad [4]$$

where γ_1 and γ_2 are the surface energies of the solids and γ_{12} the interfacial energy. Replacing the A_{12}/z_0^2 term in Eq. 4 from Eq. 2 gives,

$$F_0 = 2\pi R(\gamma_1 + \gamma_2 - \gamma_{12}) \quad [5]$$

or, if both materials are the same,

$$\gamma_1 = \gamma_2 = \gamma \text{ and } \gamma_{12} = 0$$

so that,

$$F_0 = 4\pi R \gamma \quad [6]$$

This was first derived by Bradley (10) using pairwise summation.

Assuming that contact between smooth, small diameter fibers can be treated as a "single asperity" contact^b, the analysis of the adhesion data then resolves to that of two curved elastic bodies in

^b Single asperity contact indicates that the apparent and actual areas of contact are equal.

contact. The strength of the adhesive junction will be determined by a balance between the surface attractive forces and bulk elastic forces opposing deformation. Two theories have been proposed to describe such a contact. The first is due to Derjaguin, Muller and Toporov (DMT) (11-13) which was developed for hard materials. They suggested that under the action of attractive forces the solid is deformed according to the Hertzian equation for the elastic deformation of solid surfaces. The attractive force produces a finite area of contact and is balanced by the corresponding elastic forces in the contact zone as shown in Fig. 2. If an external load P is applied the area of contact is increased. However, since all the deformations in this model are reversible the area returns to its equilibrium value when the applied force is removed. If a negative load is applied, the area of contact diminishes and the pull-off force (F) reaches its maximum value,

$$F = 2\pi R\Delta\gamma \quad [7]$$

when the contact area just reaches zero.

An alternative approach was proposed by Johnson, Kendall and Roberts [14] who suggested that the DMT analysis ignores modification of the Hertzian deformation by surface forces. They postulate that for low modulus solids such modifications play an important part in deformation and adhesional behavior. It is found that under the action of surface forces the surfaces are drawn together and a finite area of contact of radius a_0 is established for zero applied load. However, the shape is quite different from that associated with Hertzian deformation in having a small neck around the contact zone. From the Johnson-Kendall-Roberts (JKR) model the pull-off force (F) is,

$$F = \frac{3}{2}\pi R\Delta\gamma \quad [8]$$

The pull-off force is thus comparable with, but smaller than that given by the DMT model. Figure 2 shows the interaction between a sphere and a hard flat surface and the contact radius according to the DMT and JKR theories. The DMT theory is probably more applicable to the work reported here since the distortion of the Hertzian contact area is likely to be small for high modulus fibers as suggested by Pashley et al (15).

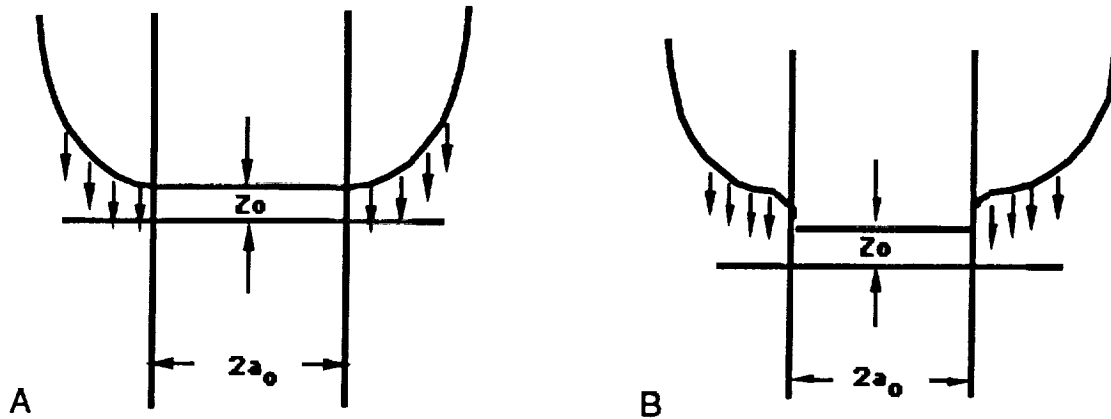


Figure 2 - Illustration of the contact deformation according to the DMT (A) and the JKR (B) theories.

Friction: If two solid bodies are placed in contact under a normal load N , a finite force is required to initiate and maintain sliding; i.e., static and dynamic friction respectively. There are two classical laws of friction for solid surfaces in contact. The first law states that the frictional force F is proportional to the load N acting perpendicular to the surfaces,

$$F = \mu N \quad [9]$$

where μ is the coefficient of friction. The second law states that the frictional force is independent of the geometric area of contact of the bodies that are sliding against each other. These relations, known as "Amontons-Coulomb's law" [16] of dry sliding friction, are used as guide lines in tribological applications. Moreover, they assert that the coefficient of friction is always about 0.3 and this is in fact about the usual value if there is no wear involved. Tomlinson (17) made an interesting attempt to correlate the molecular interaction during sliding of two unlubricated solids. He considered that the friction was due to the energy dissipated when the molecules were forced into each other's atomic fields and were then separated. He made the further assumption that the molecular fields of force were approximately the same for all substances, and the area of molecular contact could be calculated from Hertz's equation for elastic deformation. This molecular nature of friction was elaborated by Bowden and Tabor (1) and Achard (18) and led to a simple form for the friction coefficient,

$$\mu = \frac{\tau}{P_0} \quad [10]$$

as the ratio of the shear strength of microjunctions, τ , to the yield pressure, P_0 , where yielding refers to shear deformation of the softer material. In this model, Bowden and Tabor suggested that surface asperities adhere to form junctions and the frictional force is directly related to the force needed to shear these junctions. The normal load (N) is supported by the total contact area A of the elastically and plastically deformed asperities. If τ is the shear strength of the adhesive junctions, then the frictional force F is given by

$$F = A \tau \quad [11]$$

They also included another contribution to the frictional force, Ψ , due to the ploughing of the softer material by hard asperities. Thus, the total frictional force consists of two terms, an adhesion term $A\tau$ (shear yielding from adhesion forces) and a ploughing term Ψ ,

$$F = A\tau + \Psi \quad [12]$$

The principal results of Bowden and Tabor's model are reasonable. However, the model is too simple to be very useful. It is based on the assumption of homogeneous and isotropic materials, it uses a limited number of variables, and the parameters involved are somewhat ambiguous. Despite the considerable amount of work that has been devoted to the study of friction since these early investigations, there is no simple model to predict or to calculate friction of a given pair of materials. However, it is obvious that friction originates from complicated molecular-mechanical interactions between contacting bodies. Tabor (19) pointed out that there are three key factors that determine the friction between unlubricated solids;

- (a) the actual area of contact between the sliding surfaces,
- (b) the type and the strength of bond that is formed at the interface where contact occurs, and
- (c) the way in which the material in and around the contacting regions is sheared and ruptured during sliding.

MATERIALS AND EXPERIMENTAL PROCEDURES

Materials: Silica fibers were flame drawn from 2mm diameter rods (California Quartz Co., Santa Ana, CA). Table I summarizes some physical properties of these silica rods. Silica fibers having diameters in the range 25 to 35 μm were formed by drawing the silica rod in an oxygen/natural gas flame at about the softening temperature of silica (1300°C). Care was taken to ensure that the rods were always placed in the same position in the flame. In this way the rods experienced reasonably constant temperature and chemical conditions. Fibers were produced by a double-draw technique. The rod was first drawn or 'necked' locally to about half the original diameter and the final fiber drawing carried out from the necked portion.

Table I Typical Properties of Fused Quartz^c

Density	2.2x10 ³ kg/m ³
Tensile Strength	48x10 ⁶ N/m ²
Compressive Strength	641x10 ⁶ N/m ²
Bulk Modulus	3.7x10 ⁹ N/m ²
Young's Modulus	70x10 ⁹ N/m ²
Hardness	9.8x10 ⁹ N/m ²
Shear Strength	70x10 ⁶ N/m ²
Poisson's Ratio	0.17
Softening Point	1670°C
Dielectric Properties at 293 K and 1MHz:	
Dielectric Constant	3.75
Dielectric Strength	7x10 ⁴ V/m
Index of Refraction	1.4585

Figures 3A and 3B show typical scanning electron micrographs of the freshly drawn fiber. Note that the surface of the fiber is very smooth at a magnification of 12,000 (Fig. 3A). The fibers were also circular as seen from the cross-sectional view (Fig. 3B).

^c California Quartz Co., Santa Ana, CA 92704

ORIGINAL PAGE
BLACK AND WHITE PHOTOGRAPH

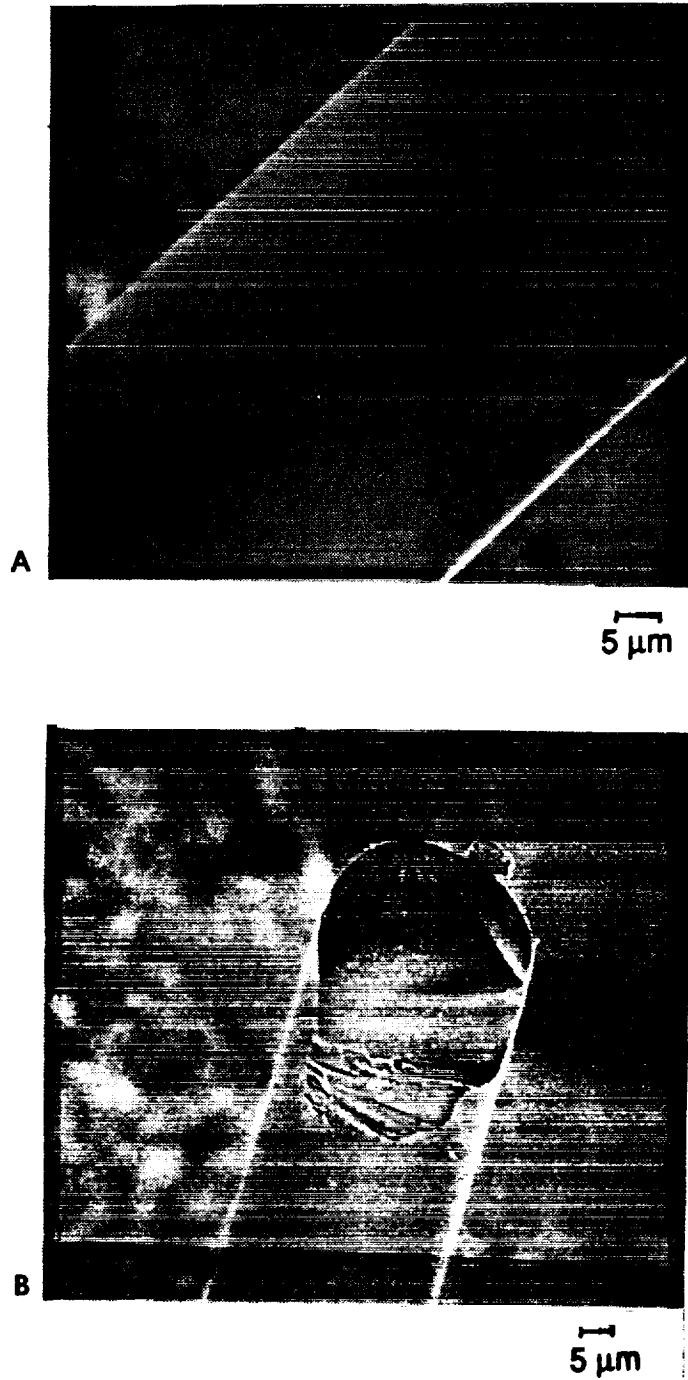


Figure 3 - Scanning electron microscopy photographs of flame drawn silica fibers. The fiber surface is smooth (A) and has an essentially circular cross section (B).

Friction and adhesion measurements were made in three liquids, n-hexadecane, cyclohexane and water. Hexadecane and cyclohexane were purchased from Aldrich Chemical Co. (Evanston, MN). Hexadecane was used as received without further purification (>95%). Cyclohexane was purified by passing through a column containing florisil (60-100 mesh) which was activated by heating at 200°C for 2 hours. The cyclohexane was used immediately after purification. Deionized water was further purified by passing through a Technic Central Lab Five Water Purification System (Seattle, WA) after which the water conductivity was 10^{18} (Mohm-cm)⁻¹ or less. Freshly drawn fibers were put into each liquid prior to adhesion or friction testing. In the case of water, the time of immersion in water was varied in order to determine the effect of surface hydration on friction. The fibers in hexadecane and cyclohexane were kept in a closed container over molecular sieve for 12 hours. The fibers were removed from the liquids using clean (acetone rinsed) tweezers and mounted in the enclosed experimental chamber (see below) and allowed to dry for no more than 30min prior to testing.

Adhesion Measurements: The adhesion measurements and the friction measurements discussed in the next section were all made using an electromicrobalance (Cahn Instrument Co. Cerritos, CA Model 2000) with a force sensitivity of 5×10^{-9} N and a motor driven support platform (Rame-Hart, Mountain Lakes, NJ) that could be moved in the vertical direction at rates of 5 to 12 $\mu\text{m/sec}$. The experimental procedure for the adhesion (pull-off) force measurements involved a pair of silica fibers in an orthogonal configuration as shown schematically in Fig. 4. The upper fiber, in the form of a loop, was held by an alligator clip which was machined to a small enough size so that its weight could be tared out using the electronic balance controller. The alligator clip was hung on a hook at the end of the thin metal wire connected to the balance. This wire passed through a non-magnetic stainless steel tube to protect it from air drafts.

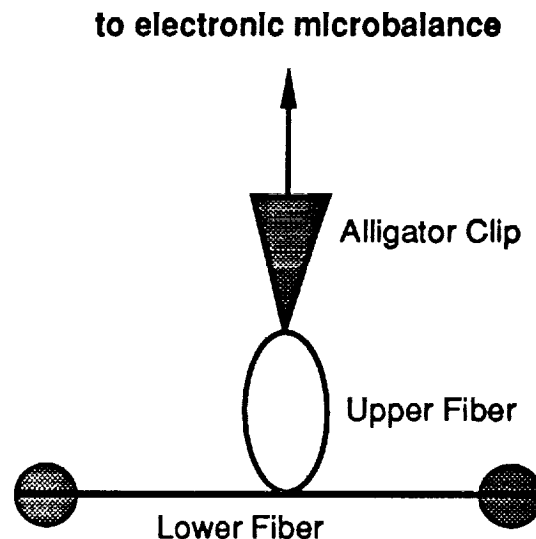


Figure 4 - Schematic of the fiber configuration used in the adhesion experiments. One fiber was in the form of a loop suspended from the electrobalance. The other fiber was held on a movable platform using the device shown in Fig. 5.

Figure 5 shows a device which was developed to hold the horizontal fiber for both the adhesion and friction measurements using minigrabbers made of non-magnetic stainless steel. The device was placed on a precision mechanical stage that could be moved up or down at preset speeds. A platform speed of $6.7 \mu\text{m}/\text{sec}$ was used for the whole range of experiments unless otherwise specified. The fiber holder could also be moved in the horizontal direction using a manual driven micrometer stage. The entire unit, fiber holders, positioning table and motors were enclosed in a transparent plastic enclosure for protection from air drafts and aerosol contamination. The equipment was placed on a vibration-free bench and most experiments were done at night when building vibrations were minimal.

ORIGINAL PAGE
BLACK AND WHITE PHOTOGRAPH

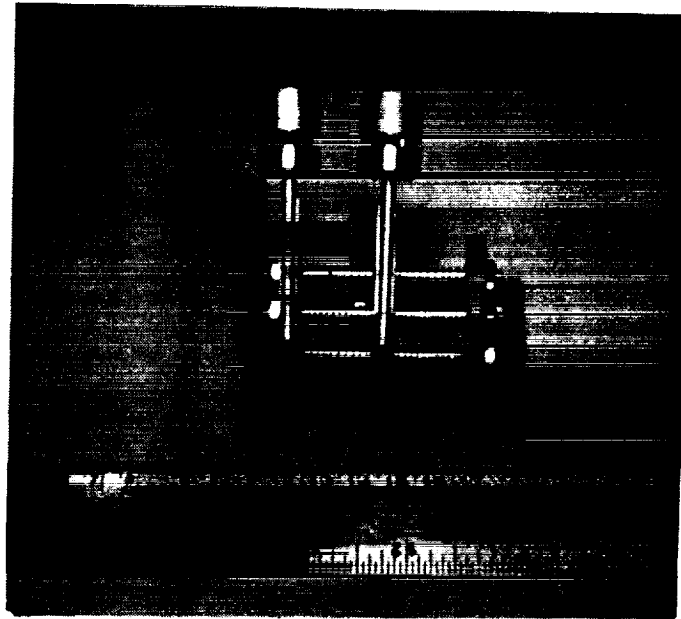


Figure 5 - Device used to hold the horizontal fiber in both the adhesion and friction measurements. Two stainless steel minigrabbers are mounted on spring loaded rails so that the distance between the minigrabbers can be varied to adjust the tension on the fiber.

Control of the tension on the horizontal fiber was critically important in both the adhesion and friction experiments. The device shown in Fig. 5 was constructed so that the distance between the minigrabbers could be varied to adjust the tension on the fiber. This procedure was somewhat arbitrary in that the tension could not be measured. However, through trial and error, it was found that the experiments were repeatable if the fiber was made just slightly taut by a few turns of the screw mechanism used to adjust the distance between the grabbers. The moment of contact and separation of the two fibers were monitored using a telescope.

To measure the pull-force, N_a , the lower fiber was brought into contact with the upper fiber. Once in contact, the motion of the platform was reversed and the pull-off force was measured at the moment of detachment of the lower fiber. The output from both the electronic balance and the stage displacements were either plotted on an XY recorder or fed into a computer (Zenith Data Systems PC) which was interfaced with the balance through an analog/digital converter (DASH-8, Metrabyte, Taunton, MA). Data acquisition was performed using Lab-Tech Notebook software (Laboratories Technology Co., Wilmington, MA) and the sampling rate was set at

10Hz. The collected data were analyzed using the Lotus 1-2-3™ program. A typical trace for a pull-off force measurement is shown in Figure 6, where the force is plotted as a function of the travelling distance. The maximum was taken as the pull-off force for a pair of fibers. The measurements were done at several locations along the horizontal fiber for each fiber pair. A total of 9-10 measurements were made and the results averaged.

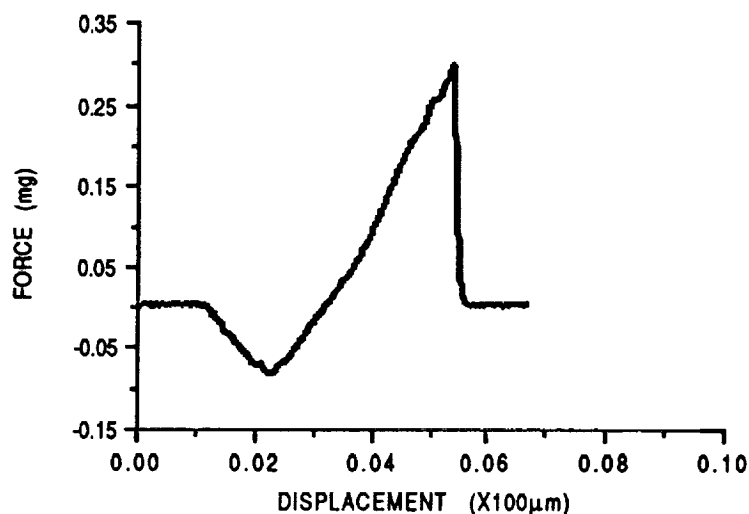
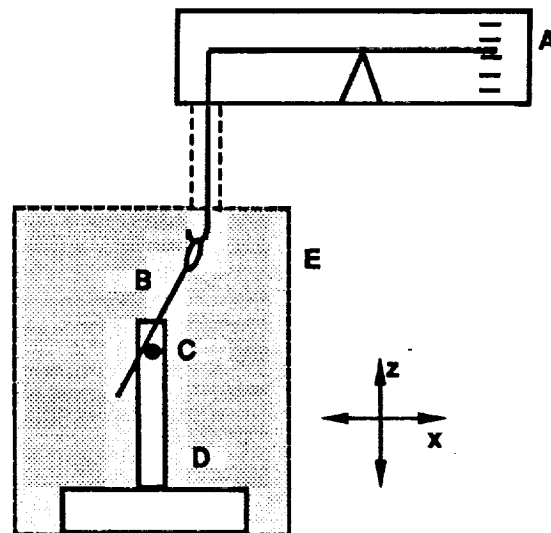


Figure 6 - Typical trace of pull-off force

Friction Measurements: The experimental procedure for the friction measurements involved a pair of silica fibers in an orthogonal configuration in which a horizontally fixed fiber is pushed against the vertically hanging fiber to apply a normal load (Fig. 7), and the frictional force was measured when the horizontal fiber was pulled down against the vertical fiber. The vertically hanging fiber (approx. length 6 cm) was again held using alligator clips and the horizontal fiber was held using the device shown in Fig. 5. Friction measurements were made by first weighing the vertical fiber including the support wire and the alligator clip. The measured weight was recorded and tared out using the electrobalance controller. Next the horizontal fiber was moved against the vertical fiber until the latter was displaced a distance d and was at an angle θ to the vertical direction as shown in Fig. 8. The angle θ was measured using a telescope fitted with a goniometer eyepiece. The

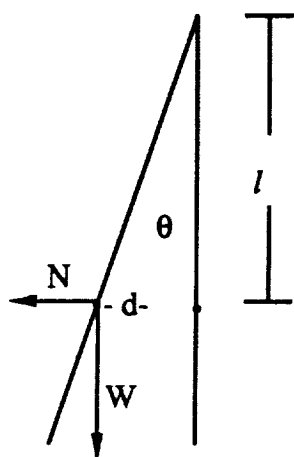
™ Lotus Development Corp, Cambridge MA

force of the vertical fiber against the horizontal fiber (N) was calculated using the expression given in Fig. 8. The horizontal assembly was then moved up and down against the hanging filament and the resulting frictional force recorded. For a downward movement, the recorded weight is the frictional force, F_d . Upward movement of the horizontal fiber caused a bending and lifting of the vertical fiber so friction data were collected only from the downward stroke. The normal load (N) was controlled by changing the angle of deflection of the vertical fiber and the range of angles was kept small ($1-6^\circ$) so that the change in angle of the vertical fiber during an experiment was negligible. For the maximum angle of deflection, the variation of angle during motion was at most $\pm 0.04^\circ$. The total sliding distance along the vertical fiber was 3mm. Friction measurements of silica monofilaments were made both in air and in the liquids and Table II lists these experiments. Fibers were tested in air after soaking in hexadecane and cyclohexane to determine if exposure to these liquids affected the frictional behavior compared to flame drawn silica.



- A. Microbalance
- B. Vertical Fiber
- C. Horizontal Fiber
- D. Platform
- E. Enclosure

Figure 7 - Schematic of the test configuration used for friction measurements.



$$\tan \theta = \frac{d}{l} = \sin \theta$$

$$N = W \sin \theta$$

Figure 8 - Displacement of the vertical fiber and the relationships between displacement and the normal force (N) at the point of contact.

Table II
Experimental Conditions for Adhesion and Friction Tests

FIBER	EXPERIMENTAL CONDITION
flame drawn	in air
flame drawn and held in water for 6hrs (23°C)	in air in water
flame drawn and held in hexadecane for 6hrs (23°C)	in air in hexadecane
flame drawn and held in cyclohexane for 6hrs (23°C)	in air in cyclohexane

An α -particle radiation source was positioned near the fiber contact region to minimize surface charging in all the adhesion and

friction experiments. All testing was done at constant relative humidity (20%) and temperature (23°C).

Adhesion and Friction Measurements in Liquids: For the adhesion and friction measurements in liquids, the horizontal fiber holding fixture was immersed in a glass container which had a flat window through which the fiber pair could be viewed. The container was filled so that the contact point between two fibers was fully immersed. The liquid was replaced for every measurement to avoid cross contamination. The horizontal fiber holding fixture and the glass container were cleaned using a mixture (20:1 by volume) of deionized water and Laboratory Cleaning Solution (International Production Co., Trenton, NJ) at 70°C and dried with clean, dry nitrogen gas. As in the experiments with dry fibers, the sliding speed was 6.7 $\mu\text{m/sec}$. which was slow enough to avoid hydrodynamic effects.

Contact Angle Measurements: Contact angles of various liquids against the silica fibers were measured using the Wilhelmy balance. In the Wilhelmy balance technique (20) the fiber is suspended from the electrobalance and immersed and emerged through the surface of the test liquid. The contact angle (θ) is given by,

$$F_w = p \gamma_{lv} \cos\theta \quad [13]$$

where p is the perimeter of the fiber along the three phase boundary line and the other terms have their usual meaning. Calculation of θ requires an independently determined value for the liquid surface tension, γ_{lv} . In addition to the wetting force, any significant immersion of the fiber in the liquid results in a buoyancy force F_b acting on the fiber. However, buoyancy forces are not significant for thin diameter fibers as evidenced by the fact that the measured force was constant with increasing immersion and emersion depth.

The cleanliness of the fibers was determined by measuring the contact angle for water (72.6 mJ/m^2), hexadecane (27.5 mJ/m^2), and cyclohexane (25.5 mJ/m^2) at room temperature (22°C) on freshly drawn silica fibers. Table III summarizes the results. We would expect that the contact angle for all three liquids

Table III
Wettability of Flame Drawn Silica Fibers

	Contact Angle (θ°)	
	advancing	receding
water	31.8	11.9
hexadecane	3.3	0
cyclohexane	5.6	2.8

on flame drawn silica should be zero. The fact that the observed contact angles were finite, suggests some low level contamination probably introduced during the manipulation of the fibers from flame drawing to mounting on the microbalance.

DATA ANALYSIS

In nearly all of the experiments reported here, the static friction was greater than the kinetic friction. Consequently, the fibers did not move smoothly against one another but, instead, exhibited a "stick-slip" motion as shown in Fig 9. Figure 10 shows a schematic of the friction data. The motion is not steady but consists of fluctuations in which the pull on the vertical fiber increases steadily (AB) and then falls very rapidly (BD). When the horizontal fiber moves, the fibers are sticking together for the time interval between A and B. Consequently, the force at the maximum B is the static friction (F_s). At B a rapid slip of the vertical fiber occurs and when the force has fallen to D the surfaces stick together again .

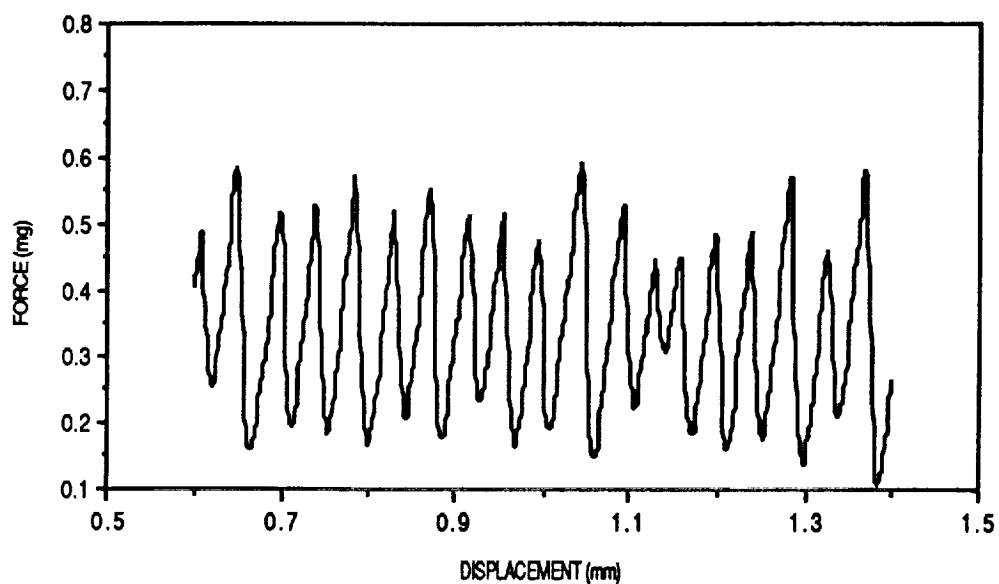


Figure 9 - Typical force displacement trace for two flame drawn silica fibers in air.

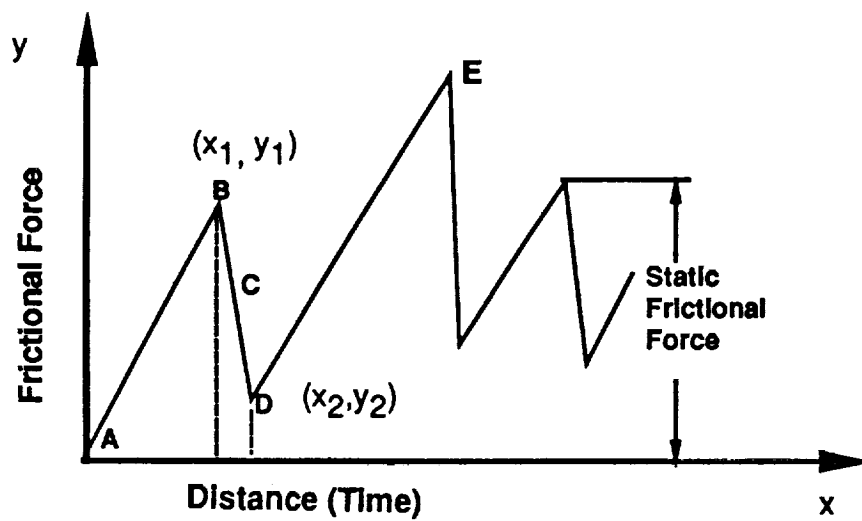


Figure 10 - Schematic force-distance curve for stick-slip frictional response.

Consider a simple idealized experiment that simulates the sliding friction of two solid bodies in contact (Figure 11). A post C is fixed to a stationary flat bed (M). The movable plate B is mounted

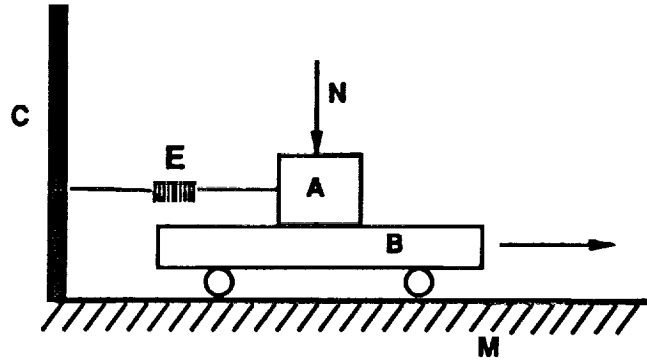


Figure 11 - Diagrammatic representation of slip-stick motion

on frictionless rollers. Resting on plate B is the block A under a normal load N. The block A is restrained by the spring E, one end of which is fastened to the post C and the other to the block. When plate B moves in the direction indicated by the arrow, it carries with it the block A, thereby extending the spring. At some critical force the block is no longer carried along by the plate but instead slides in the reverse direction. Initially, the magnitude of the adhesive force between the block and plate is greater than the force exerted by the restraining spring so that the block will be carried along by the plate so that the spring extension corresponds to the initial slope (AB) in Figure 10. At a distance x_1 , corresponding to the arrival of the block at position B, a rapid slip occurs and the block moves back in the reverse direction, which slows it down, and at x_2 the block sticks to the plate again and is carried along with it as indicated by DE in Figure 10. Thus, as the driven surface moves steadily forward, the motion of the block is a series of alternate sticks and slips. The behavior of the block along BD can be analyzed exactly. The equation of motion of the surface in free oscillation and, assuming there is no damping, is,

$$m \frac{d^2x}{dt^2} = -kx \quad [14]$$

where m and k are the mass of the moving block and the spring constant, respectively. Thus the motion is a simple harmonic of frequency n ,

$$n = \frac{1}{2\pi} \sqrt{\frac{k}{m}} \quad [15]$$

If the block A has an applied load of N , the surfaces travel together without relative motion until the force on the free surface is equal to the static friction, $F_s = \mu_s N$. The deflection to x_1 is linear with time and equal to $(\mu_s N)/k$. At point B slip will occur and we may assume, as a first approximation, that the kinetic friction during the slip has a constant value $F_k = \mu_k N$. The equation of motion of the surface is now modified to,

$$m \frac{d^2x}{dt^2} - \mu_k N = -kx \quad [16]$$

where, at x_1 (point B), the deflection is,

$$x_1 = (\mu_s N)/k$$

and the forward velocity dx/dt is equal to v . The solution for Eq. [16] is,

$$x = \frac{N}{k} \{ (\mu_s - \mu_k) \cos \omega t + \mu_k \} + \frac{v}{\omega} \sin \omega t \quad [17]$$

where $\omega = \sqrt{k/m}$. If the velocity of the lower surface is small compared with the mean velocity of the slip, the last term in Eq. 17 may be neglected so that,

$$x = \frac{N}{k} \{ (\mu_s - \mu_k) \cos \omega t + \mu_k \} \quad [18]$$

Thus the motion of the free surface has the same natural frequency as before and it comes to rest relative to the lower surface, that is, it sticks again when $dx/dt = v$. If v can be neglected we may consider that sticking recurs when $dx/dt = 0$, i.e. when $\omega t = \pi$. This is half the natural period of the system and by inserting this value of ωt in equation [18] we find that,

$$x = (2\mu_k - \mu_s)N/k.$$

Thus the length of the slip , $\overline{x_1x_2}$, is,

$$(2\mu_s - 2\mu_k)N/k$$

From this relation, the larger μ_k the smaller the slip. In the limit when $\mu_k = \mu_s$ the slip becomes zero, so that the deflection remains steady at B. This condition corresponds to the case of smooth sliding. As μ_k decreases slip-stick behavior intensifies.

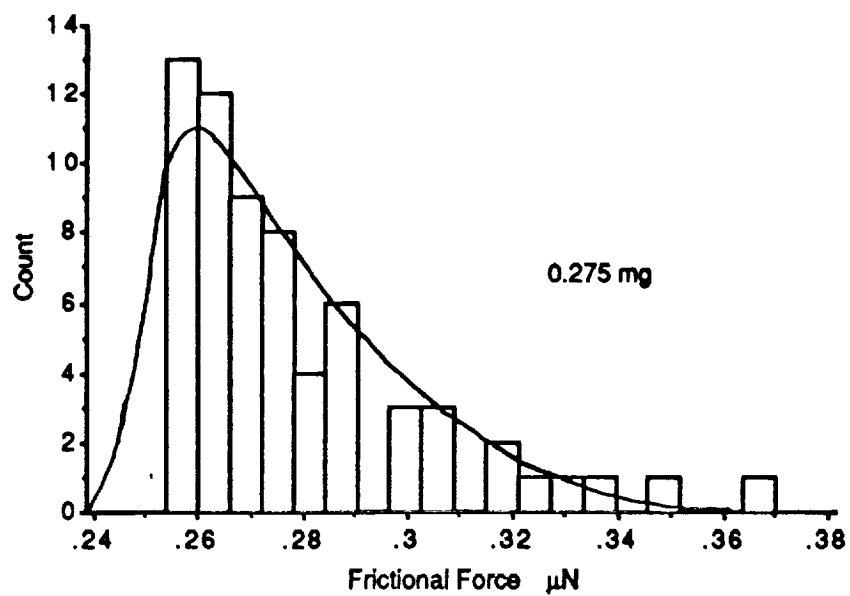
The distance of the mid-point C of the slip from zero is simply equal to $\frac{1}{2}(\overline{x_1x_2}) = \mu_k(N/k)$. Therefore, the deflection at the end of the stick (point B) corresponds to the static friction μ_s , while the mid-point of the slip (point C) corresponds to the kinetic friction μ_k . It would appear that data from this study could yield information on kinetic as well as static friction. However, the main interest here is the static frictional force values, i.e., the peak heights.

The maxima of the data from the friction measurements were collected using a macro program for Lotus 1-2-3. The arithmetic mean M and variance s^2 of the static frictional forces were calculated from the following expressions.

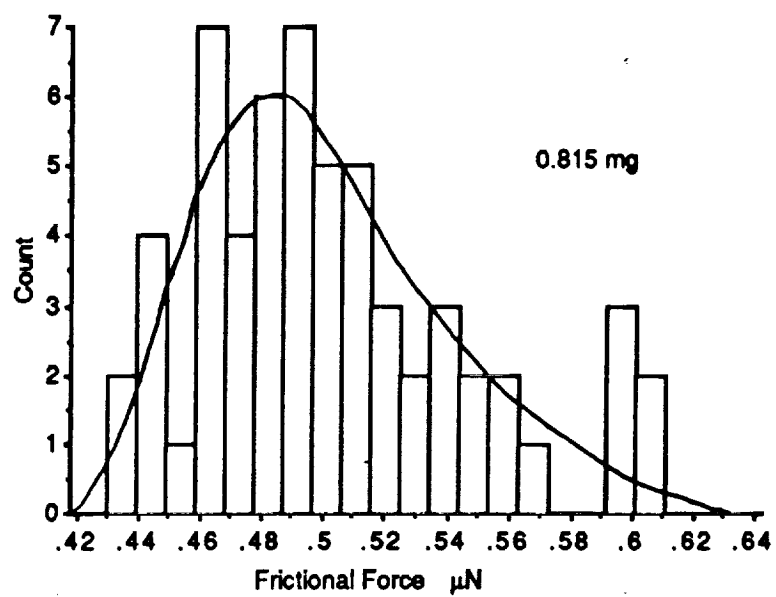
$$M = \frac{1}{N} \sum_{i=1}^N F_i \quad [18]$$

$$s^2 = \frac{1}{N-1} \sum_{i=1}^N (F_i - M)^2 \quad [19]$$

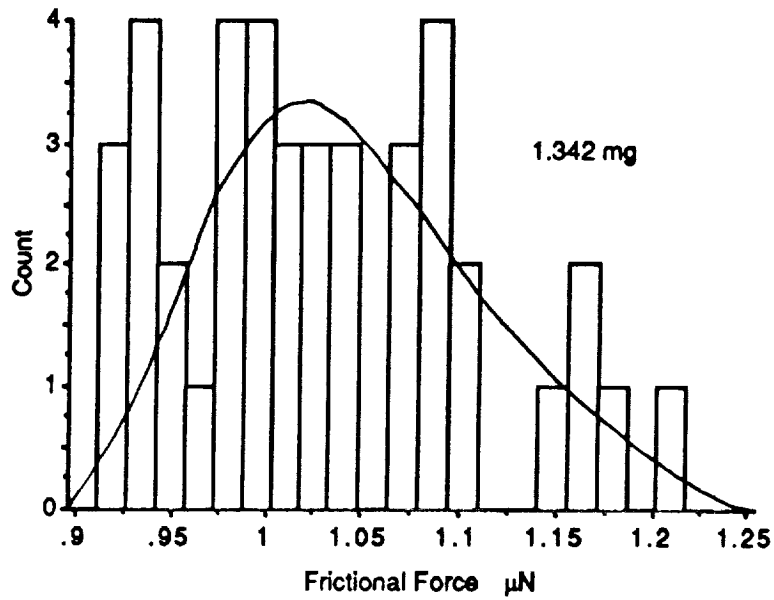
Frequency distributions at different loads are plotted in Fig. 12. At low loads the curve rises steeply to a relatively high peaked



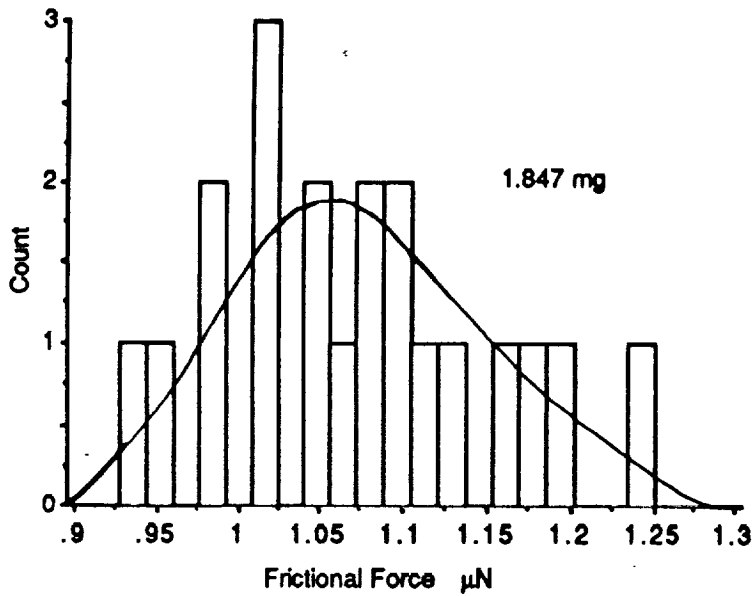
A



B



C



D

Figure 12 - Histograms of static friction data for silica fibers tested in air at normal forces of 0.27mg (A), 0.815mg (B), 1.342mg (C) and 1.847mg (D).

modal value after which it decays sharply with a short tail. As the load increases the maximum decreases and the tail becomes longer. For small values of applied normal load, an exponential probability distribution curve is suggested, as shown in Figure 12A. In general the exponential density function is given by (21),

$$f(x) = \frac{1}{\theta} e^{-x/\theta} \quad x \geq 0 \quad [20]$$

$$= 0 \quad \text{elsewhere}$$

where the parameter θ is an applied normal load that determines the rate at which the curve decreases and x is the observed static frictional force. Only a small portion of the friction data could be fit by an exponential function; mostly data taken at low loads. It was more common to see distributions with low probabilities at intervals close to zero and the majority of the data having a skewed distribution (Fig. 12B). This type of behavior is characterized by the gamma distribution with the gamma probability density function given by,

$$f(x) = \frac{1}{\Gamma(\alpha)\theta^\alpha} x^{\alpha-1} e^{-x/\theta} \quad x > 0 \quad [21]$$

$$= 0 \quad \text{elsewhere}$$

where x is the observed static frictional force. The parameters α and θ determine the specific shape of the curve and they are determined from the observed x values. Note that the gamma density function reduces to the exponential when $\alpha = 1$. Further increase in the normal load is accompanied by a systematic change in frequency distribution until the normal distribution is approached (Fig. 12C).

$$f(x) = \frac{1}{\sqrt{2\pi}} \sigma e^{-(x-M)^2/2\sigma^2} \quad [22]$$

where, $-\infty < x < \infty$

M = mean

σ = standard deviation

None of the distribution functions would fit all of the data.

Table IV summarizes the statistical data for the load conditions in Fig. 12. Note the increase in the mean frictional force with increasing applied load. This trend suggests that junction breakdown is increasingly difficult as the applied normal load is increased.

Table IV
Effect of Normal Load on the Slip-Stick Frequency
Distribution Parameters

Load (μN)	Mean Force (μN)	Std. Dev. (μN)	Variance (μN)	Count	Skewness
0.28	2.73	0.24	0.00	65	1.49
0.82	4.93	0.43	0.01	59	0.70
1.32	10.1	0.76	0.06	41	0.51
1.85	10.7	0.81	0.07	20	0.21

RESULTS AND DISCUSSION

Adhesion and Friction of Dry Fibers in Air: The contact adhesion results are listed in Table V.

Table V
Contact Adhesion Results

Experimental conditions	Pull-off Force (μN)	Std. Dev. (μN)
fresh fiber in air	4.97	0.46
fiber equilibrated* in water and tested in air	3.10	0.84
fiber equilibrated* in water and tested in water	1.70	0.42
fiber equilibrated* in hexadecane and tested in air	1.15	0.1
fiber equilibrated* in hexadecane and tested in hexadecane	0.24	0.08
fiber equilibrated* in cyclohexane and tested in air	2.97	0.07
fiber equilibrated* in cyclohexane and tested in cyclohexane	0.052	0.000

* fibers were immersed in each liquid for 6hrs.

Figure 13 shows the results of adhesion measurements for freshly drawn silica fiber where the pull-off forces are plotted as a function of fiber radius. The pull-off force, N_a , is directly proportional to the fiber radius R (Eqs. 7 and 8). The value of γ deduced from the slope of the linear regression line is 34.4 mJ/m^2 using the DMT theory. This is an unexpectedly low value for the surface energy of fresh silica since it has been shown from extrapolation of the data for the surface energy of molten alkali silicate glasses (22) that the approximate value for the surface energy of silica in air should be at least 200 mJ/m^2 . Evidently, there must be strong short range repulsive forces at separation distances of a few nanometers. This conclusion is consistent with work by Israelachvili and Tabor (23) and Johnson et. al. (14) that the adhesion between solids are primarily the result of van der Waals' force interactions. Similar results in terms of the surface energy have been reported by Kohno and Hyodo (24) for the contact adhesion between fused quartz and an optically flat steel surface.

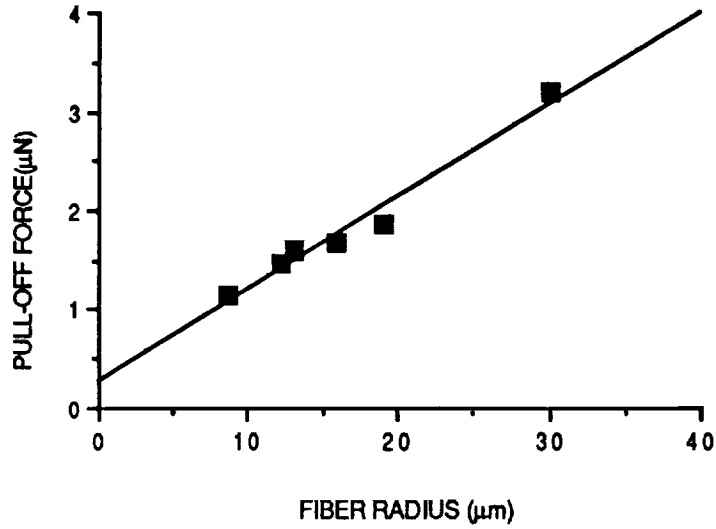


Figure 13 - Pull-off force vs fiber radius for freshly drawn silica fibers.

It is instructive to compare the measured pull-off force with the non-retarded van der Waals interaction force. As discussed earlier, the force interacting between two bodies is given by Eq. 1 where it is assumed that the interaction is nonretarded and additive. However, the assumptions of simple pairwise additivity inherent in Eq. 1 and the definition of the Hamaker constant ignore the influence of neighboring atoms on the interaction energy. In rarefied media these effects may be small, and the assumptions of additivity hold but this is not the case for condensed media. This problem of additivity is completely avoided in the Lifshitz theory where atomic structure is ignored and the forces between large bodies, now treated as continuous media, are derived in terms of such bulk properties as dielectric constants and refractive indices. For two identical phases, 1, interacting across medium, 3, the Hamaker constant is given by (25),

$$A = A_{v=0} + A_{v>0} = \frac{3}{4}kT\left(\frac{\epsilon_1 - \epsilon_3}{\epsilon_1 + \epsilon_3}\right)^2 + \frac{3h\nu_e(n_1^2 - n_3^2)^2}{16\sqrt{2}(n_1^2 + n_3^2)^{\frac{3}{2}}} \quad [35]$$

where $A_{v=0}$ is the purely entropic zero-contribution and $A_{v>0}$ is the

dispersion energy contribution. From Eq.1, z is given a constant minimal value z_0 which is the distance between the outermost centers of polarization of the two nearest atoms belonging to the two bodies. The value $z_0 \cong 2\text{nm}$ is a good approximation as discussed by Newman et. al. (26). Table VI summarizes the Hamaker constants based on Eq. 1 with experimentally observed pull-off forces and the calculated values using Eq. 35 based on the constants given in Table VII. There is good agreement between the Hamaker constants measured and calculated for air as the medium. The agreement breaks down completely for the values in liquid media.

Table VI

Comparison of the Hamaker Constants for Silica Fiber in Different Environments Based on Pair-Wise Interactions (Eq. 1) and Continuum Theory (Eq. 33)

Test Media	Pull-Off Force (μN)	A (10^{-20}J)	
		Eq. 1	Eq. 33
air	4.97	6.28	6.3
water	1.702	3.4	0.63
hexadecane	0.240	0.3	0.03
cyclohexane	0.052	0.07	0.03

TABLE VII

Material Constants used in Calculating the Hamaker Constants from Eq, 33

	Dielectric Constant	Refractive Index	Absorption Frequency ($10^{15}/\text{sec}$)
fused quartz	3.8	1.148	3.2
water	80	1.333	3.0
hexadecane	2.04	1.423	2.9
cyclohexane	2.9	1.426	2.9

We are especially interested in estimating the surface shear strength from the static friction measurements. The contact area may be calculated using the Hertz analysis with the normal load (N)

taken as the sum of the applied load (N^*) and adhesive force (N_a). The shear strength is given by,

$$F = \tau A \quad [22]$$

where τ and A are the interfacial shear strength and real area of contact, respectively. This expression is the same as Eq.11 but without the ploughing term which is not pertinent for these studies.

The actual area of contact may be a function of the normal force since it is known that when plastic materials are brought into contact, increasing the contact force may lead to an increase in the true contact area as a result of irreversible deformation (27, 28). In order to address this question the adhesional force was measured at increasing pressing forces ($0.01\mu\text{N}$ - $3\mu\text{N}$) and it was found that the force varied by less than 5% so we are able to ignore changes in the contact area with applied load.

From the theory of Hertz (29) for the contact of two spherical bodies within the elastic limit, the area of contact and the pressure p at any radii within the contact area are given by,

$$a = \sqrt[3]{\frac{3NR}{4E'}} \quad [23]$$

$$p = \frac{3N}{2\pi a^2} \left(1 - \left(\frac{r}{a} \right)^2 \right)^{1/2} \quad [24]$$

where N is the applied load, R the equivalent radius of curvature given by,

$$\frac{1}{R} = \frac{1}{R_1} + \frac{1}{R_2} \quad [25]$$

and E' is the composite elastic modulus defined by,

$$\frac{1}{E'} = \left\{ \frac{1-\nu_1^2}{E_1} + \frac{1-\nu_2^2}{E_2} \right\} \quad [26]$$

where E_1 , E_2 are the Young's moduli for the elastic bodies, ν_1 and ν_2 their Poisson's ratios, and R_1 , R_2 their radii of curvature, as shown in Figure 14. Since the contact area $A = \pi a^2$, the area of the contact circle is,

$$A = \pi a^2 = \pi(NRK)^{2/3} \quad [27]$$

where K is a constant,

$$K = \frac{3(1-\nu^2)}{2E'} \quad [28]$$

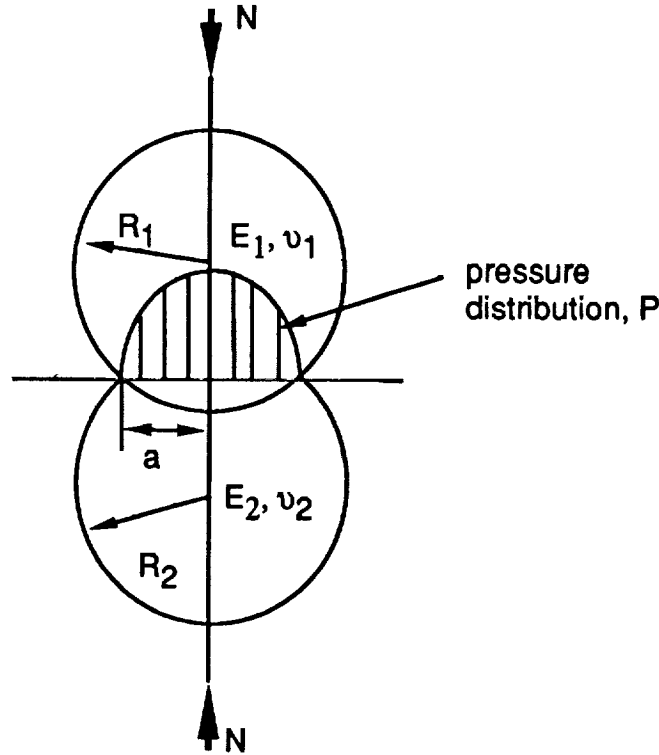


Figure 14 - Schematic of the the contact area between two fibers under a normal load N.

Figure 15 shows the frictional force as a function of normal load for freshly drawn silica fibers in air. Each data point is the mean of at least three measurements of different sets of fiber pairs. The coefficient of friction, μ , decreases from about 10 at low loads to 5.2 at $2\mu\text{N}$.

For single asperity contact the friction data should fit the equation,

$$F = MN^{0.7} \quad [29]$$

which is obtain from Eqs 22 and 27,

$$F = \tau\pi(NRK)^{2/3}$$

$$F = \tau\pi(RK)^{2/3} N^{2/3}$$

$$M = \tau\pi(RK)^{2/3}$$

From Fig. 15 the load exponent (n) is 0.69. Winkler et. al. [10] also found that $n = 0.7$ for the sliding of polyethylene terephthalate fibers against glass fibers.

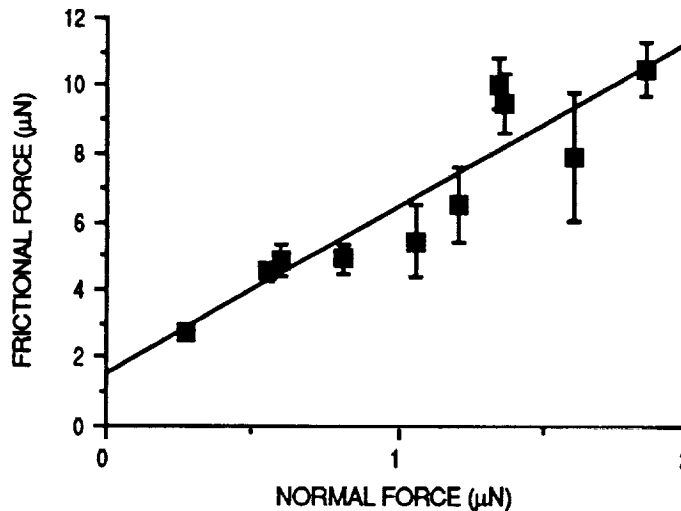


Figure 15 - Applied normal force vs frictional force for freshly drawn silica fibers.

Extrapolation of the friction force to zero applied load results in a finite applied load which, in principle, corresponds to the adhesion force between the fibers. In Fig. 15, the frictional force was 2.1 μN at zero applied load. Ideally, this frictional force should be identical to the "pull-off" adhesional force, (4.97 μN , Table III) for freshly drawn fiber in air. The latter is significantly higher. Similar differences between the two forces were observed by Derjaguin and Toporov (30). They point out that contact adhesion is measured when the normal load is taken off whereas the value obtained from friction measurements depends on the relief of elastic stresses so that the two experimental conditions are not equivalent. This difference between sliding contact and normal contact is also discussed by Savkoor and Briggs (31) for an elastomer half-sphere sliding against a glass plate.

In Fig. 16 the shear strength (τ) is plotted as a function of the applied pressure and τ ranged between 0.05 and 0.25 GPa. The details of the calculation are given in the Appendix. These values of the surface shear strength are significantly less than the measured value of the bulk shear strength of 70GPa (Goodfellow Metals Cambridge Ltd., Cambridge, England) for fused quartz. The theoretical shear strength, τ_t , of silica was calculated from the elastic engineering constants using Eqs. 30 and 31,

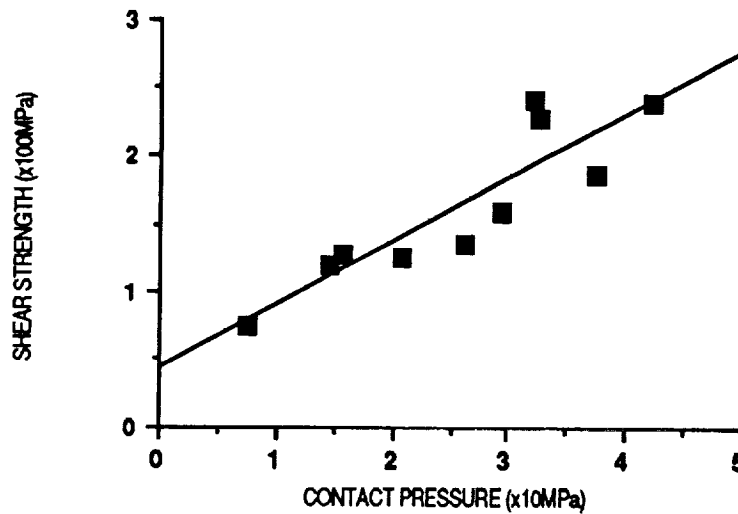


Figure 16 - Pressure dependence of the shear strength for silica fibers in air.

$$G = \frac{E}{2(1+\nu)} \quad [30]$$

$$\tau_t = \frac{G}{2\pi} \quad [31]$$

where G , E and ν are the shear modulus, elastic modulus and Poisson's ratio respectively. For $E = 70$ GPa and $\nu = 0.24$ for silica, G is 28.2 GPa. From Eq. 31 the theoretical shear strength is 4.5 GPa, an order of magnitude greater than obtained here. King and Tabor (32) determined the strength properties and frictional behavior of various types of glass from friction measurements and found that

the surface shear strength of glasses to be of the order of 1.4 GPa again higher than measured here.

Differences between the experimental results reported here and from theory are not unexpected. The high level of defects in experimental materials compared to the defect free material assumed in theoretical calculations results in an over estimation of the shear strength. As for the experimental results of King and Tabor, the structure of the glass near the surface will depend on how the test specimen was made; e.g. flame drawing vs polishing. The low shear strength value obtained here for flame drawn fiber suggests that near the surface the silica has a low density or is highly defective at a microscopic level. The fact that τ increases with applied pressure suggests that this defect structure is collapsing with increasing load.

Friction Measurement in Liquids: Figure 17 compares the frictional behavior between freshly drawn fiber tested in air and in water. The good lubrication efficiency between silica/silica in water is probably the result of a weakly bound film of water molecules adsorbed on the fiber surface. With the assumption that the mechanical properties of the fiber near the surface do not change significantly in water, the interfacial shear strength was 110 MPa which is somewhat lower than for the dry fibers. Presumably, water acts as a boundary lubricant and also reduces the adhesive component of the normal load. Figure 18 shows the frictional behavior of silica fiber in air as a function of hydration time. There were no measurable differences in the friction data for hydration times of 1-6 hours. However, after prolonged soaking of the silica fibers (10 days), the frictional force increased significantly. This can be ascribed to surface degradation due to water attack probably resulting in a gel-like structure on the surface. Degradation of the fiber surface after 10 days in water could be seen using scanning electron microscopy (Fig. 19). The softening of the surface leads to an increase in the area of contact and increased friction and possibly ploughing of the surface.

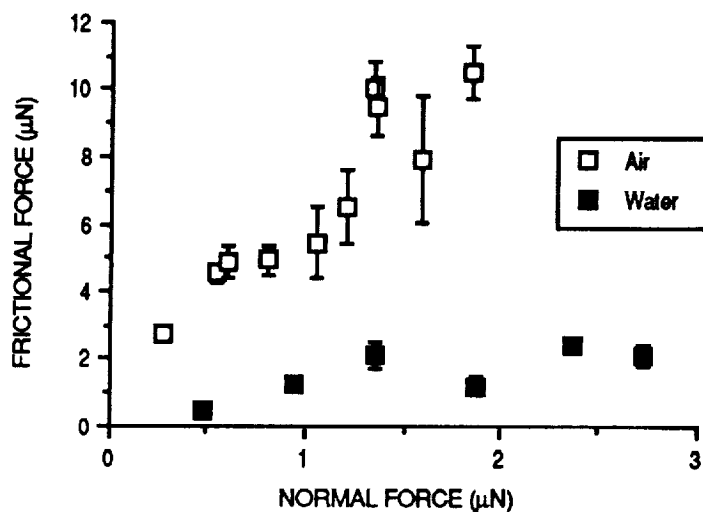


Figure 17 - Frictional behavior of freshly drawn silica fiber in air and in water.

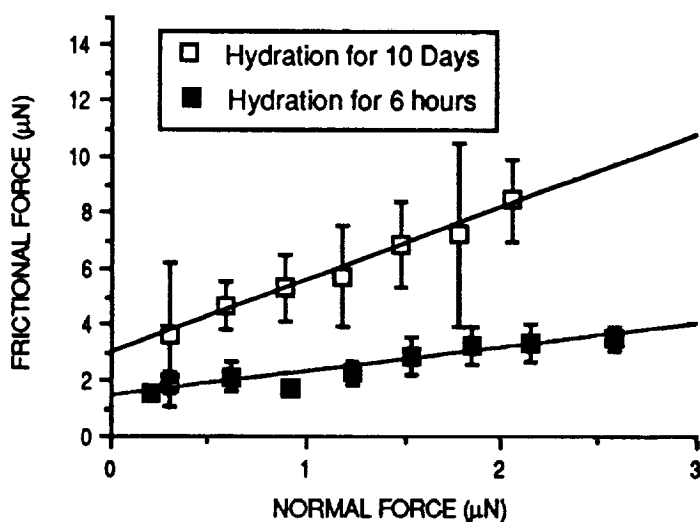
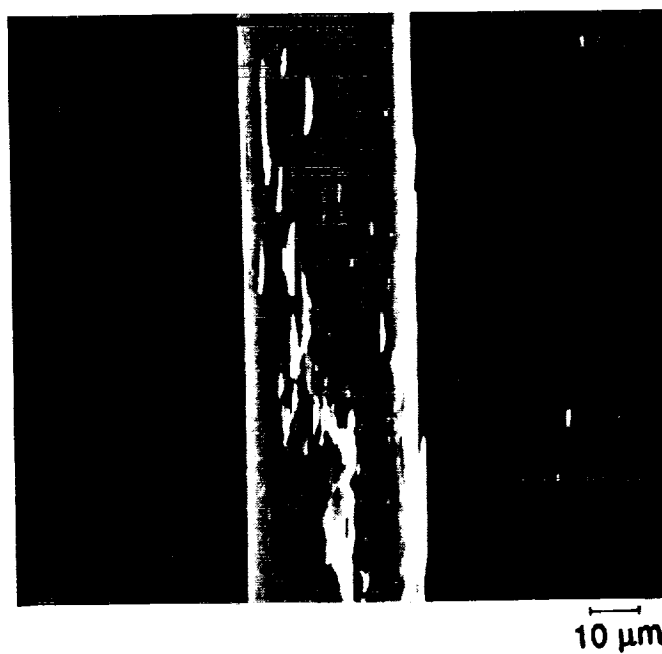


Figure 18 - Effect of prolonged hydration on the friction of silica fibers. The results for 6hrs. hydration are essentially identical to those for fibers tested in water immediately after drawing.



ORIGINAL PAGE IS
OF POOR QUALITY

Figure 19 - Scanning electron micrograph of a silica fiber after soaking for 10 days in water.

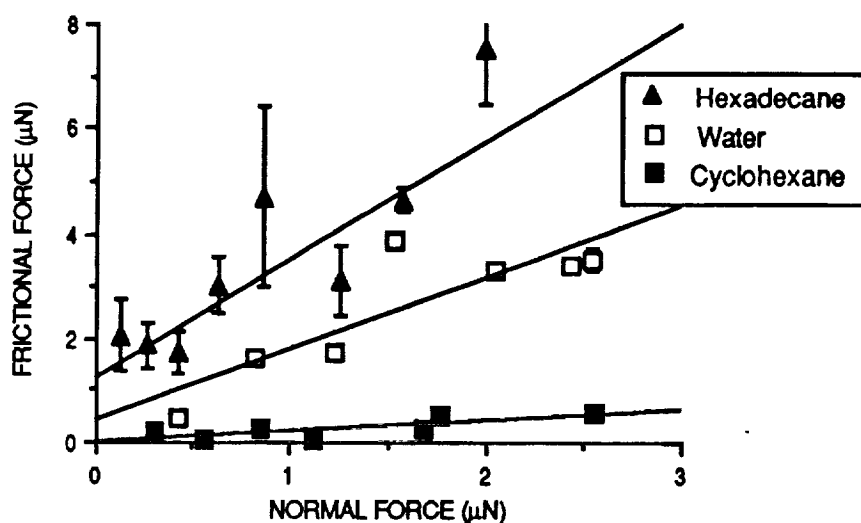


Figure 20 - Comparison of the friction of silica fibers in water, hexadecane and cyclohexane.

Figure 20 compares the frictional behavior of silica fibers in water, hexadecane and cyclohexane and the data indicate several phenomena. In hexadecane the friction was significantly higher than in water which supports the suggestion that adsorbed water has a "lubricating" effect on the frictional behavior of silica. The most interesting observations were those made in pure cyclohexane. It

would appear that cyclohexane acts as a boundary lubricant in these tests. This conclusion is supported by the data in Table V where it is shown that the adhesional force between silica fibers in cyclohexane is very low. This significantly reduced friction (and adhesion) in cyclohexane may be a result of the formation of a stable film of liquid molecules on the fiber surfaces.

Typical traces of the frictional behavior in the three liquids are presented in Fig. 21. In contrast to the fiber in air (Fig. 9), the slip-stick motions in hexadecane and water were highly erratic which explains the large data scatter shown for hexadecane in Fig. 20. In order to reduce the scatter, a procedure was adopted to exclude peaks less than 60% of the maximum peak height based on the assumption that at these lower points the fibers had not made complete contact.

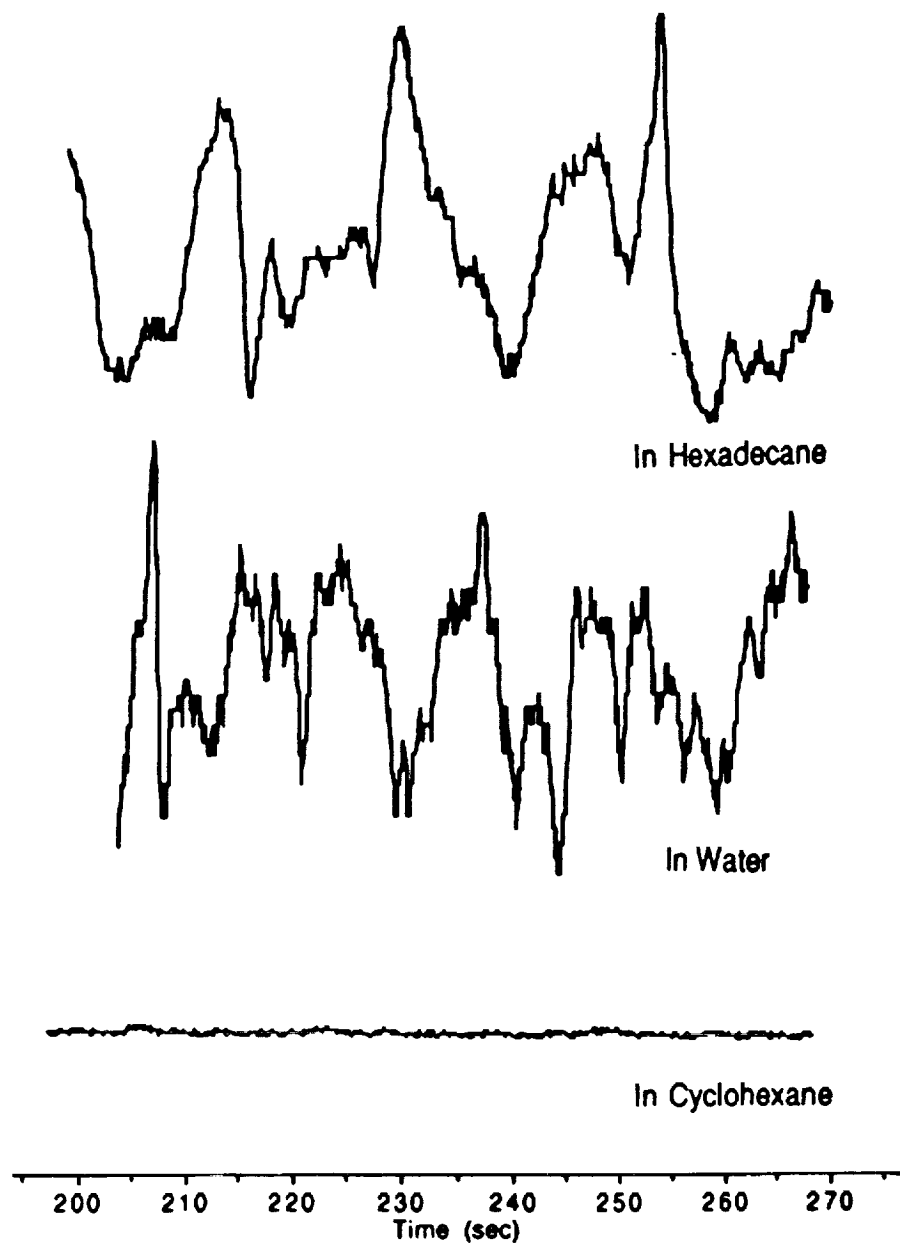


Figure 21 - Friction traces for silica in hexadecane, water and cyclohexane.

The trace for cyclohexane in Fig. 21 is consistent with the low friction of the silica fibers in this liquid (Fig. 20). It would appear that the cyclohexane acts as a boundary lubricant. Israelachvili et al. (33) observed that the force between two curved mica surfaces immersed in cyclohexane over a few nm (approximately 10 molecular diameters) is spatially oscillatory, i.e., varies between attraction and repulsion, with a periodicity equal to the molecular size. These rapidly decaying oscillatory forces indicate that the molecules are layered near the surfaces, and this layering prevents the surfaces from coming into adhesive contact. This observation is consistent with the pull-off force results (Table V) and with the low friction.

The effects of contact pressure on the surface shear strengths are compared for silica fibers tested in air and in water in Fig. 22. As expected from the lower frictional forces in water (Fig. 16), the shear strength is significantly lower in water than in air. To some degree, the water molecules at the fiber surfaces are acting as a boundary lubricant.

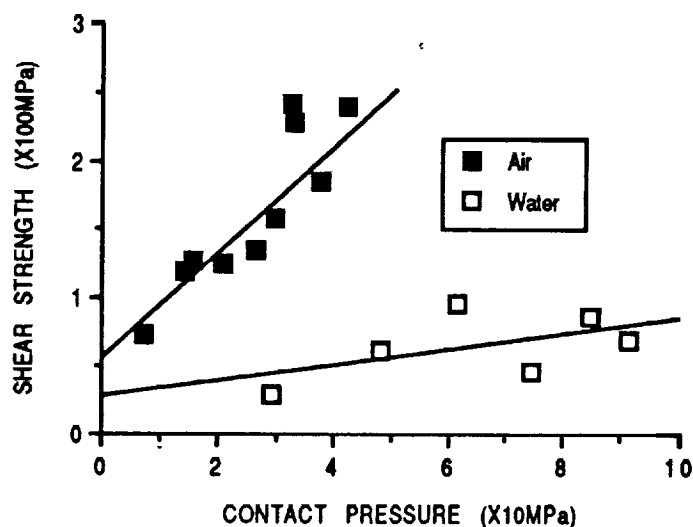


Figure 22 - Shear strength vs contact pressure for silica fibers tested in air and in water.

CONCLUSIONS

Silica fibers flame drawn from commercial quartz rod had a circular cross-section 25-35 μ m in diameter. Scanning electron microscopy showed a smooth surface at a magnification of X12,000 which supports our assumption that the contact between the two

fibers is single point contact. When these fibers are placed orthogonally against one another they experience a finite adhesion due to surface forces. These forces can be expressed in terms of surface energies. It was found that the measured pull-off forces as a function of fiber radius was linear. The surface energy values were obtained from the slope of the linear regression line of pull-off force vs fiber radius using the DMT analysis. The value obtained was 34.4 mJ/m². While this is very small compared with the estimated surface energy of silica fibers, it is reasonably close to the interaction due to van der Waals' forces.

In the friction experiments, the fibers were slid against one another and the friction depended on the load, N . The motions were intermittent "stick-slip" and when the static frictional forces were plotted as a function of the applied load, it was found that there is a simple relationship $F = W^n$ where n is the order of $2/3$. This suggests that contact occurs at a single point so that the area of contact can be calculated using Hertzian contact deformation mechanics.

From a statistical analysis of the friction data it was found that the distribution function of the static frictional force could be described by the exponential, gamma, and normal distribution functions depending on the normal contact load.

If the friction is due primarily to shearing at the interface, we may write $F = A\tau$ where τ is the interfacial shear strength and A varies with the normal load to the $2/3$ power. Calculations based on single point contact give values of τ of the order of 0.05 - 0.25 GPa. Observed shear strength of the bulk quartz was 70 GPa and an experimental estimate of the surface shear strength of silicate glasses was 1.4 GPa. The much lower shear strength of the silica fibers tested here is attributed to a highly defective surface structure.

When freshly drawn silica fibers were hydrated for 1 to 6 hours, differences in the friction and adhesion were not statistically significant. However, when the fiber was hydrated for 10 hours, the friction was increased up to a factor of 3. This effect is probably due to a formation of a gel-like structure at the fiber surface thus increasing the area of contact.

When the friction was measured in hexadecane, the frictional forces were as high as the frictional forces for the fresh fiber in air. However, in the case of cyclohexane, a marked reduction in friction was observed and this result was attributed to the formation of an adsorbed boundary layer.

PART II: FRICTION AND ADHESION OF SILICA FIBERS COATED WITH ADSORBED ORGANIC MONOLAYERS

BACKGROUND

The ability of strongly adsorbed monolayers of organic molecules to reduce the adhesion and friction of metals and inorganic solids is well established (7, 34). These films act as boundary lubricants and usually are amphipathic molecules having a strongly polar group(s) that bond to the metal or inorganic substrate and a weakly polar group that extends away from the surface to reduce the sliding friction. Commercial compounds of this type are added to motor oils to provide boundary lubrication when bearing parts are too close together to allow the oil to provide hydrodynamic lubrication. These additives are complex organic compounds but their action can be simulated by relative simple molecules such as long chain aliphatic (n-alkyl) amines and carboxylic acids and by long chain aliphatic (n-alkyl) silanes. In this study, these model adsorbate molecules are used since there are well established techniques for applying them to silica surfaces to form strongly adsorbed, closely packed monomolecular films.

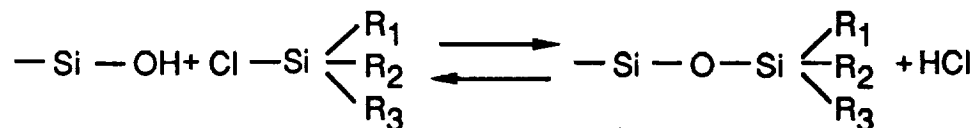
MATERIALS AND FILM PREPARATION

Materials: The adsorbates were n-octadecylamine (Aldrich Chemical Co.), trimethylmonochlorosilane (TMCS, Petrach System Inc.) and n-octadecyldimethylmonochlorosilane (DMODCS, Petrach System Inc.). They were used as obtained from the suppliers. The solvents from which octadecylamine was adsorbed were hexadecane and cyclohexane. The surface energy of the adsorbed amine is low enough that both hexadecane and cyclohexane retract from the fibers as they are removed leaving a dry surface having an adsorbed monolayer coating (35). The alkyl silanes were applied from toluene (36). The solvents (hexadecane, cyclohexane and toluene) were reagent grade materials (>99% purity). Hexadecane was used as received. The cyclohexane and toluene were purified by passing through a column containing florisil (60-100 mesh) which was activated by heating at 200° C for 2 hours before use.

Film Preparation: Solutions containing 0.1 wt% octadecylamine were prepared in hexadecane and cyclohexane at 60° C in a glass container. Before preparing the solutions, all the glass

containers were cleaned using a mixture (20:1 by volume) of deionized water and Laboratory Cleaning Solution (International Products Co.) at 70° C. They were then rinsed with hot tap water and a large amount of distilled and deionized water and blown dry with clean, dry nitrogen. Freshly drawn silica fibers were immersed in each solution and kept for 24 hours over a molecular seive desiccant in a covered container. In retracting a monolayer of octadecylamine from hexadecane or cyclohexane, it is possible to produce a mixed film of solute and solvent molecules. Consequently, the fibers were immersed for 24 hours in an effort to minimize entrained solvent (37). The fibers were then slowly retracted from the solutions using tweezers and placed in a glass jar to allow any solvent incorporated in the adsorbed films to evaporate.

Thin films of the alkyl silanes were prepared from solutions of TMCS (0.5 mole) and DMODCS (0.5 mole) dissolved in toluene. The freshly drawn fibers were immersed in these solutions for 15 minutes. The fibers were again retracted slowly from the solution using tweezers. A large amount of ethanol was poured on the fiber surface to remove any weakly adsorbed solute. The fibers were then placed in a preheated (70° C) vacuum oven for 3 hours under the gentle flow of nitrogen gas to remove residual HCl and ethanol. The HCl is produced from the reaction of the silane with surface silanols (-SiOH),



The adhesion and friction measurements were performed on these surface treated fibers using the same techniques described in the PART I. Table IX summarizes the experiments performed. Contact angles were also determined for water, methylene iodide and α -bromonaphthalene on the monolayer coatings using the Wilhelmy balance method. Critical surface tensions (γ_c) were determined using the method of Zisman (38): the value of γ_c was determined by extrapolating a linear regression analysis of the contact angle data vs the wetting liquid surface tension to $\cos \theta = 1$.

TABLE IX

Experimental Conditions for Adhesion and Friction Tests

Coating	Test Condition
octadecylamine retracted from hexadecane	in air in hexadecane
octadecylamine retracted from cyclohexane	in air in cyclohexane
trimethylmonochlorosilane retracted from toluene	in air
dimethyloctadecylmonochlorosilane retracted from toluene	in air

RESULTS AND DISCUSSION

Friction and Shear Strength of Octadecylamine Coated Fibers:

Contact angle measurements on octadecylamine (ODA) monolayers provide a good indication of how closely packed the molecules are in the adsorbed film. For comparison with previous studies (38-40) of the wettability of ODA films, the critical surface tension was determined for the films formed on the silica fibers. Table X summarizes the critical surface tension and contact angle data for the octadecylamine retracted from both hexadecane and cyclohexane. The critical surface tensions of the octadecylamine films retracted from hexadecane and cyclohexane were 20.7 and 26.6 mJ/m², respectively. The expected critical surface tension for a monolayer exposing a close-packed surface of -CH₃ groups is 22 - 24 mJ/m² (38). The critical surface tension of films from hexadecane were below this range suggesting a high packing density. However, as discussed below, this low γ_c may be due to entrained hexadecane in the monolayer. The critical surface tension for the octadecylamine film retracted from cyclohexane was significantly higher than expected for a close packed surface of -CH₃ groups which suggests that this film has a more open structure than the film formed from hexadecane.

TABLE X
Contact Angles and Critical Surface Tensions of Adsorbed
Octadecylamine Films Retracted from Hexadecane (OHA) and
Cyclohexane (OCA)

Film	$\gamma_c(\text{mJ/m}^2)$	$\theta(\text{degrees})$		
		H ₂ O	CH ₂ l ₂	α -bromonaphthalane
		adv., rec.	adv., rec.	adv., rec.
OHA	20.7	83.7, 50.6	63.4, 43.5	60.0, 46.6
OCA	26.6	80.0, 59.8	63.2, 41.6	45.7, 25.3

Figure 23 compares the frictional behavior of octadecylamine films (retracted from hexadecane) measured in air and in hexadecane. The results are essentially identical which indicates that the boundary lubrication effect of the octadecylamine film is the same in air as in hexadecane.

Figure 24 compares the frictional forces measured in air for the amine monolayer retracted from hexadecane with the film formed from cyclohexane. The frictional force of the amine retracted from the hexadecane was an order of magnitude lower than that from cyclohexane. This difference can be best attributed to the film formed from hexadecane being more close-packed than the film from cyclohexane. However, it is important to note that the film from hexadecane may include solvent molecules due to the strong dispersive attractive forces between adsorbed octadecylamine and hexadecane. Such a mixed film would present a close packed surface of -CH₃ groups. The strong attractive forces between solute and solvent molecules in the adsorbed film would resist evaporative loss of the solvent when the fibers are removed from the adsorbate solution and even after exposure to air during drying and mounting in the test apparatus.

On the other hand, adsorption of films of octadecylamine from cyclohexane would not be likely to contain co-adsorbed solvent. The molecular structure of cyclohexane prevents strong dispersion force interaction with the adsorbed solute.

These observations and comments on the frictional behavior of the octadecylamine films are consistent with their critical

surface tensions. The low γ_c of the film from hexadecane could be the result of co-adsorbed hexadecane where as the high γ_c of the film from cyclohexane could reflect a somewhat more sparse coverage.

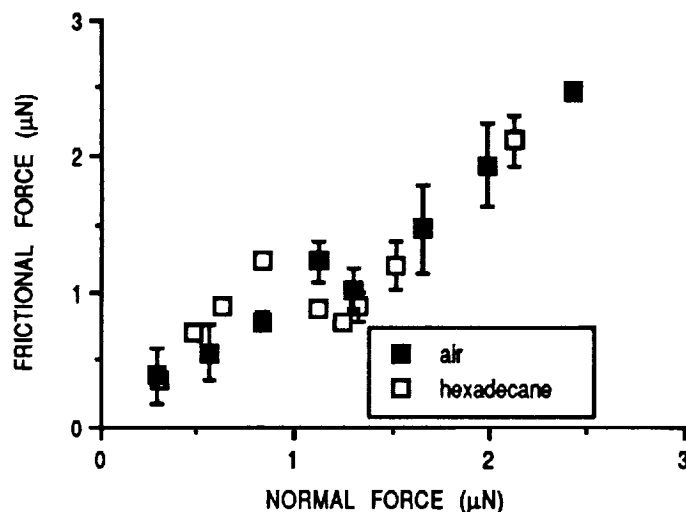


Figure 23 - Comparison of the frictional behavior of silica fibers with adsorbed octadecylamine films tested in air and in hexadecane.

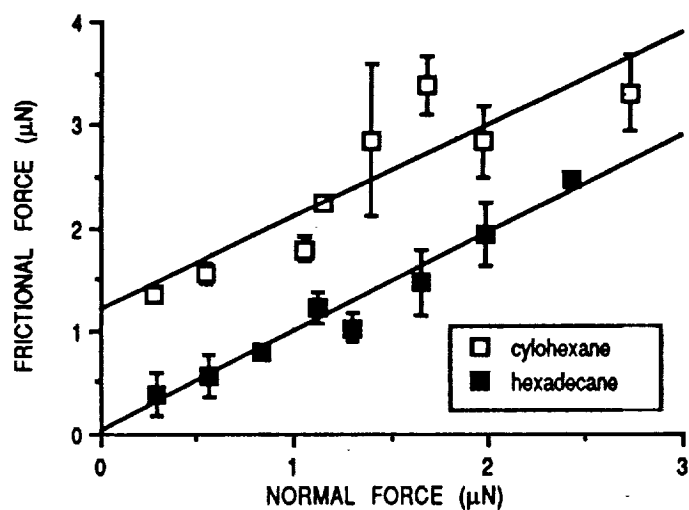


Figure 24 - Comparison of the frictional behavior of adsorbed octadecylamine on silica retracted from hexadecane or cyclohexane.

Figure 25 compares the frictional behavior of flame-drawn silica fibers equilibrated^d in hexadecane and then tested in air, and in hexadecane with the behavior of fibers with adsorbed octadecylamine tested in air and hexadecane. The effectiveness of the octadecylamine film as a boundary lubricant is clearly evident. Note, however, that the friction of the fiber equilibrated in hexadecane had been reduced significantly compared to the friction of freshly drawn fibers (Fig. 15). It is possible that equilibration in hexadecane resulted in the adsorption of some organic contamination from the solvent.

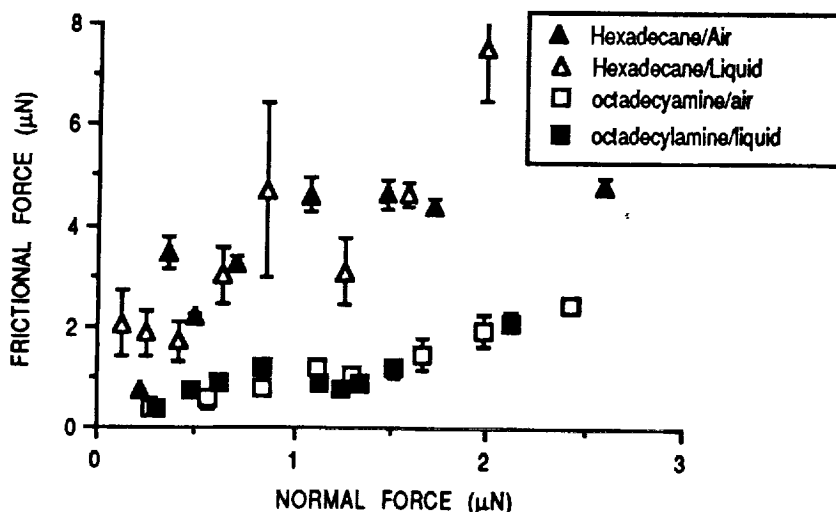


Figure 25 - Frictional behavior of uncoated silica fibers and octadecylamine coated fibers in air and hexadecane (the uncoated fibers were equilibrated in hexadecane before testing).

Figure 26 compares the frictional behavior of flame drawn silica fibers equilibrated in cyclohexane and tested in air and in cyclohexane with the behavior of fibers with adsorbed octadecylamine tested in air and cyclohexane. Equilibration of the silica fibers in cyclohexane reduced the frictional resistance in air to the same level obtained for fibers with an adsorbed film of octadecylamine retracted from cyclohexane (compare Figs. 24 and 26). The frictional resistance of uncoated fibers tested in cyclohexane was essentially the same as fibers coated with octadecylamine adsorbed from cyclohexane. It would appear that, even in air, a film of cyclohexane is present on the fiber and is an

effective boundary lubricant. In the tests in cyclohexane it would appear that the film formed by cyclohexane alone is as effective in friction reduction as an adsorbed film of octadecylamine.

Traces for the frictional behavior of silica fibers coated with octadecylamine adsorbed from cyclohexane and tested in air are compared in Fig. 27 with traces for the frictional behavior of uncoated silica fibers and fibers with an octadecylamine monolayer but tested in cyclohexane. In air, the motion was clearly stip-stick but in cyclohexane the motion was continuous. Evidently, the boundary lubrication effect of cyclohexane, discussed in PART I, is still effective when the silica surface is coated with an adsorbed film of octadecylamine.

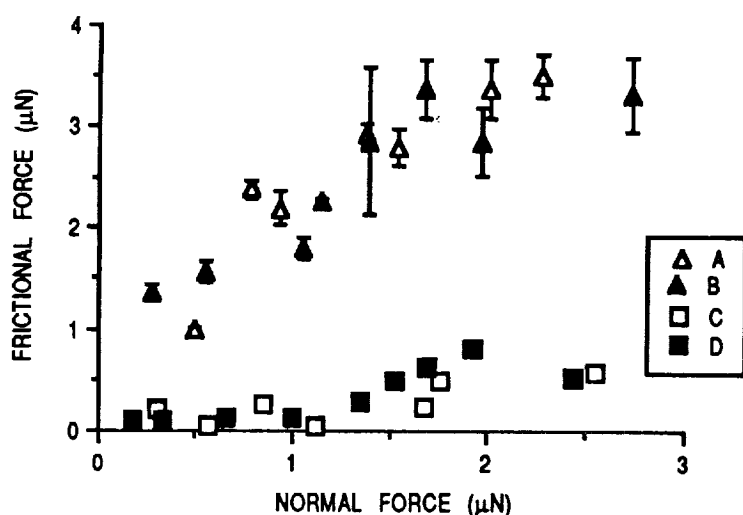


Figure 26 - Frictional behavior of silica fibers equilibrated in cyclohexane and tested in air (A), silica fibers with a monolayer of octadecylamine deposited from cyclohexane and tested in air (B), uncoated silica fibers tested in cyclohexane (C) and silica fibers with a monolayer of octadecylamine adsorbed from cyclohexane and tested in cyclohexane (D).

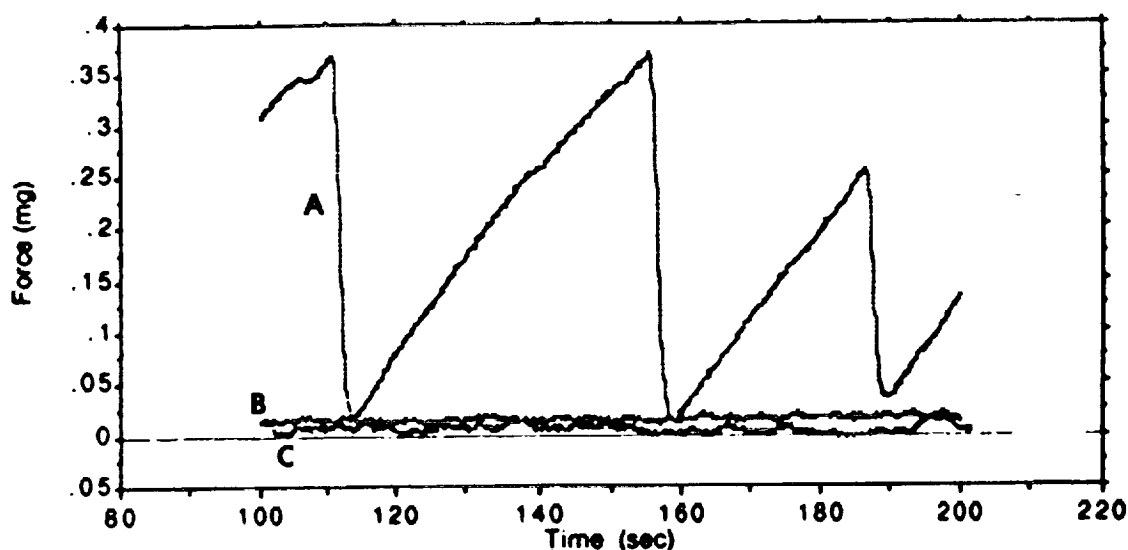


Figure 27 - Force-distance traces for silica fibers equilibrated in cyclohexane and tested in air (A) and in cyclohexane (B) and for fibers with an adsorbed film of octadecylamine from cyclohexane and tested in cyclohexane (C).

In Table XI, the pull-off forces are given for silica fibers equilibrated in hexadecane or cyclohexane and fibers with adsorbed films of octadecylamine adsorbed from hexadecane or cyclohexane. Curiously, the adsorption of octadecylamine from hexadecane resulted in a higher pull-off force than for fibers that had been simply equilibrated in hexadecane. Equally curious, is the much higher pull-off force observed for silica fibers equilibrated in cyclohexane and tested in air.

One possible explanation, albeit speculative, is that the adsorbed film of octadecylamine and the film of cyclohexane that is presumably on the fiber based on friction measurements screen the repulsive forces thereby decreasing the equilibrium contact distance, z_0 , between the fibers. If so, the adhesional force would be increased (Eq. 2).

Adsorption of an octadecylamine film from cyclohexane had no effect on the pull-off force compared to fibers equilibrated in cyclohexane. The pull-off forces for solvent equilibrated fibers measured in the solvents were low as already reported in Table V and were unaffected when coated with films of octadecylamine, at least within the sensitivity of the measurement.

TABLE XI
Pull-off Forces Measured in Air and Liquids for Fibers Treated with
Pure Liquids and with Solutions Containing Octadecylamine.

Test Condition	Pull-off Force (μN)	Test Condition	Pull-off Force (μN)
equilibrated in hexadecane, tested in air	1.2	equilibrated in cyclohexane, tested in air	3.0
equilibrated in hexadecane, tested in hexadecane	0.2	equilibrated in cyclohexane, tested in cyclohexane	0.0
octadecylamine film from hexadecane, tested in air	3.4	octadecylamine film from cyclohexane, tested in air	3.2
octadecylamine film from hexadecane, tested in hexadecane	0.2	octadecylamine film from cyclohexane, tested in cyclohexane	0.1

The surface shear strengths vs contact pressure for octadecylamine films adsorbed from hexadecane and from cyclohexane are compared in Fig. 28. As expected, the shear strengths are reduced compared to uncoated fibers (Fig. 22). Moreover, the shear strength for octadecylamine at zero applied load was 1.3 MPa which is comparable to values of 2 - 4 MPa reported for calcium stearate (42). In both cases the shear plane is between films of close-packed $-\text{CH}_3$ groups.

The higher shear strength of the octadecylamine film adsorbed from cyclohexane is probably due to this monolayer having a more open structure than the film adsorbed from hexadecane which is consistent with the higher critical surface tension of the film from cyclohexane (Table X)

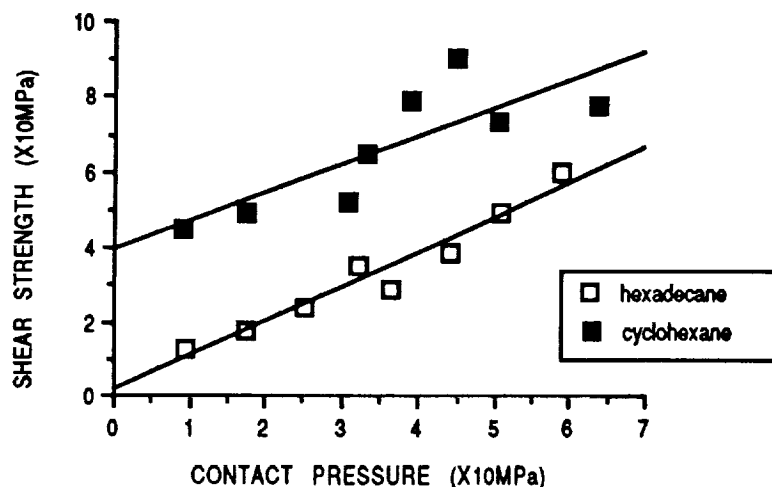


Figure 28 - Surface shear strength vs contact pressure for films of octadecylamine on silica retracted from hexadecane or cyclohexane.

Wettability, Friction and Shear Strength of Alkyl Silanes:

Films of trimethylmonochlorosilane (TMCS) and dimethyloctadecylmonochlorosilane (DMODCS) adsorbed on silica fibers were characterized by contact angle measurements in water, methylene iodide and α -bromonaphthalene. The data are summarized in Table XII. The critical surface tensions are significantly higher than for the octadecylamine films (Table X) although the contact angles for water and methylene iodide are higher than for the octadecylamine films. If we can assume that the silanes adsorb as monomolecular films in the configurations shown in Fig 29, then the TMCS films should expose a close-packed surface of $-\text{CH}_3$ groups. The DMODCS film on the other hand should have a more open structure due to the side chain methyl groups impeding close packing of the octadecylamine groups. Accordingly, we would expect the TMCS to have a lower critical surface tension than the DMOCS which is, in fact the case (Table XII) except that the absolute values are higher than expected especially for the TMCS films. Clearly, more contact angle data for other wetting liquids are needed to establish more accurate critical surface tensions.

The method used to apply the silane films was that described by Park and Andrade (44) and the contact angles they report are essentially identical to the contact angles given in Table XII.

The results of friction force measurements for TMCS and DMODCS are presented in Figure 30 which indicate significant

reductions in friction for both TMCS and DMODCS compared with fresh silica fiber (Fig. 15). The TMCS film was much

TABLE XII
Contact Angles and Critical Surface Tensions of Adsorbed TMCS and DMODCS on Silica Fibers.

Fiber	$\gamma_c(\text{mJ/m}^2)$	$\theta(\text{degrees})$		
		H_2O	CH_2I_2	$\alpha\text{-bromonaphthalene}$
		adv., rec.	adv., rec.	adv., rec.
TMCS	35.4	106, 72	68, 32	51, 33
DMODCS	39.3	99, 77	61, 43	40, 29

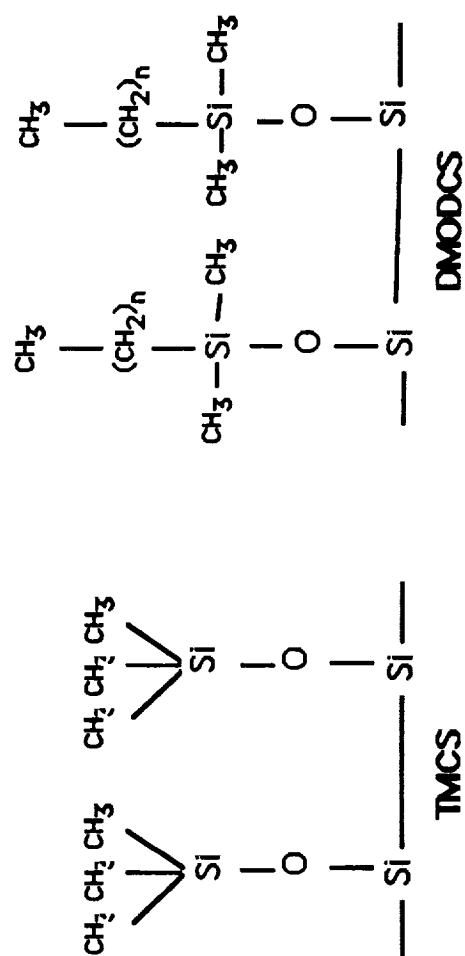


Figure 29 - Schematic of trimethylmonochlorosilane (TMCS) and dimethyloctadecylmonochlorosilane (DMODCS) molecules adsorbed on silica.

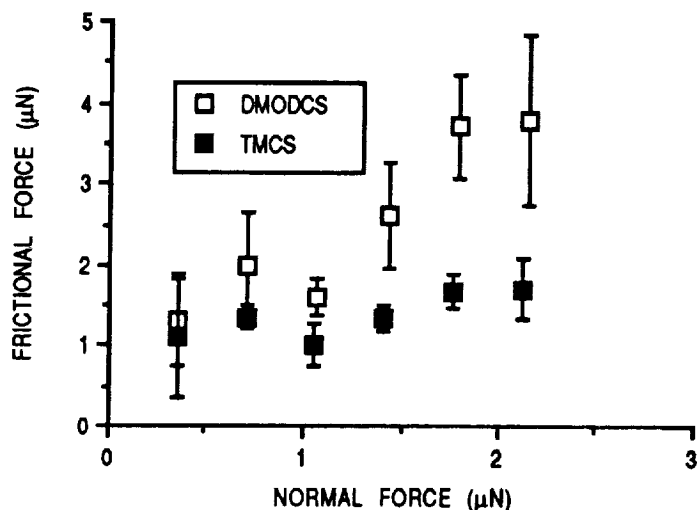


Figure 30 - Comparison of the frictional behavior of TMCS and DMODCS films on silica tested in air.

more effective in reducing friction than DMODCS. The interfacial shear strengths were calculated and are plotted against contact pressure in Fig. 31.

The pull-off forces for the silanes were surprisingly large: 6.86 and 11.76 μN for TMCS and DMODCS, respectively.

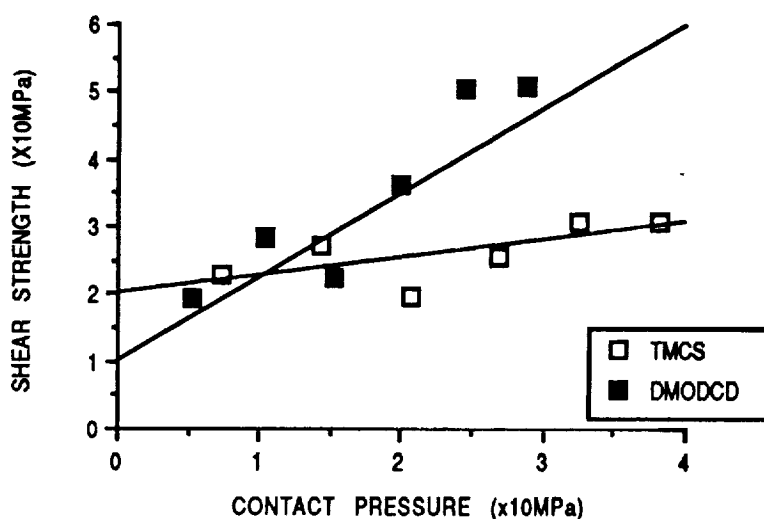


Figure 31 - Pressure dependence of the shear strength for TMCS and DMODCS films on silica

CONCLUSIONS

The adsorbed films of octadecylamine reduced the frictional resistance by as much as a factor of 10 compared to fresh fiber. The amine adsorbed from hexadecane was more effective than the film adsorbed from cyclohexane probably because the film from hexadecane was more closely packed including some co-adsorbed hexadecane. However, when tested in cyclohexane, the octadecylamine film exhibited lower frictional resistance than the film adsorbed from hexadecane and tested in hexadecane. In fact, the friction in cyclohexane was essentially identical as for uncoated fibers in cyclohexane as reported in Part I. Moreover, experimental force-distance traces indicated that in cyclohexane, with or without an adsorbed film, the motion was continuous rather than slip-stick.

The adhesional pull-off forces in air were lower for the fibers with adsorbed octadecylamine compared to uncoated, freshly drawn fibers.

Equilibrating the fibers in hexadecane and cyclohexane, without any octadecylamine, reduced the friction in air compared to fresh fibers by about 2X in the case of hexadecane and 3X in the case of cyclohexane.

The silane films also reduced the frictional forces compared to fresh fiber. In the case of the DMODCS by about 60% and in the case of the TMCS by 2X. The pull off forces for the DMODCS and TMCS were 11.8 and 6.9 μN ; some of the largest adhesional forces measured in the entire study.

PART III ADHESION AND FRICTION OF POLYMER FILMS COATED ON SILICA FIBERS

BACKGROUND

In general, the frictional behavior of polymeric materials can be understood in much the same terms used to explain the results presented in PARTS I and II. However, because of their lower shear strength and moduli the friction of polymers is different from other hard materials in at least three respects: 1) the ploughing term (Eq. 12) may constitute an appreciable part of the frictional resistance; 2) friction depends on the speed of sliding and temperature in a manner that reflects the viscoelastic properties of the polymer; 3) frictional energy is dissipated not just at the junction of the sliding surfaces but may occur to a significant depth below the surface (43, 44). The depth of this dissipation is generally of the order of 50 to 200 nm (44).

In the present study, polycarbonate (PC), polystyrene (PS) and polyethylene terephthalate (PET) films were coated on freshly drawn silica fibers and the adhesion and friction of the fibers in orthogonal contact were studied using the same methods described in PART I. Assuming that contact deformation is wholly elastic, the contact area was calculated using the classical Hertzian analysis. The interfacial shear strength between polymer-polymer contacts was estimated from the friction measurements.

EXPERIMENTAL MATERIALS AND METHODS

Polycarbonate (PC), polystyrene (PS), and polyethylene terephthalate (PET) were used as supplied (Scientific Polymer Product Inc.). The PC and PS were dissolved in tetrahydrofuran (THF, EM Sci.) and cyclohexane respectively. The PET was dissolved in a mixture of phenol and 1,1,2,2-tetrachloroethane (EM Sci.) at a 1:2 volume ratio. The solvents were heated to 70°C to facilitate solution of the polymers and the final concentration was 0.1wt% in all cases.

Polymer films from each solution were then deposited on the freshly drawn silica fibers at room temperature. The fibers were immersed for 5 minutes and withdrawn slowly using tweezers. The

coated fibers were dried in an oven at 60° C for 4 hours and then stored in a grease-free desiccator. All friction and adhesion measurements were done at constant temperature (23°C) and constant humidity (20 %).

RESULTS AND DISCUSSION

Figure 32A shows a scanning electron micrograph of a polycarbonate coated silica fiber. The film thickness was approximately 0.5 μm for all three polymer films. The coated surfaces appeared smooth at low magnifications (x1.57k) but at higher magnifications (x13.6k) none of the fibers were as smooth (Figs. 32C and D) as the flame drawn fibers. This roughness raises the possibility of multiple asperity contact. However, the assumption is made here of "single point" contact since the roughness appears to be of low amplitude and frequency and that the area of contact between fibers is small compared to the degree of roughness.

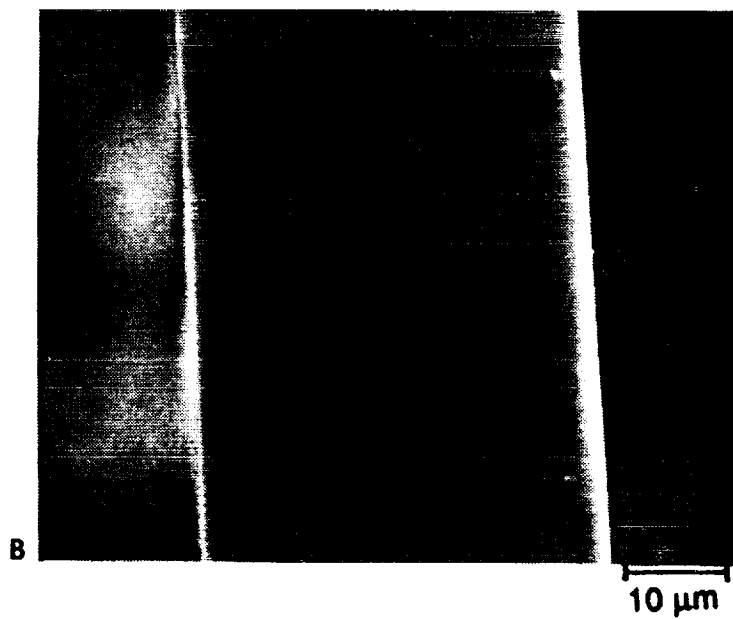
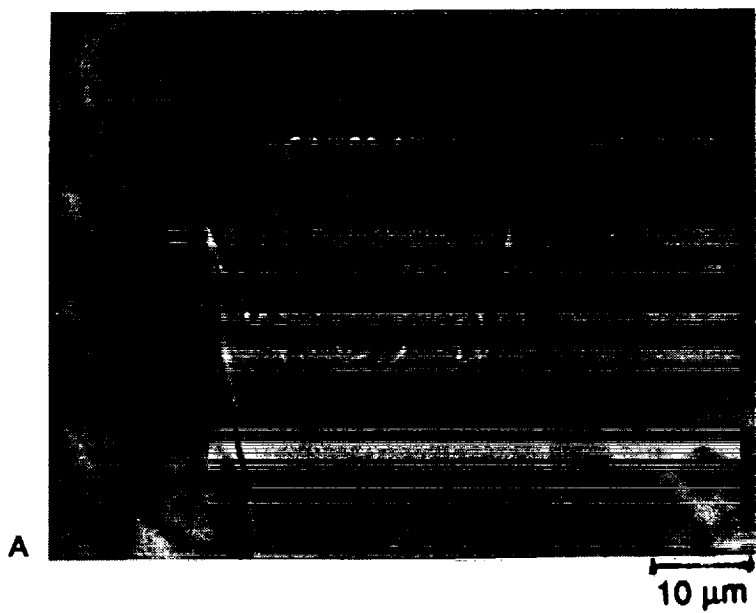
Figure 33 compares the frictional behavior of the three different polymer coated fibers in air. The friction was highest for PS and decreased in the order PS>PC>PET. Figure 34 compares the frictional force for PET coated silica fibers with that of PET monofilaments reported by Adams et al (3). Although their study was performed within a small range of applied loads, 0 to 1.25 μN , compared to 0 to 2.5 μN in the present study, the results agree very well. In Fig. 34, the frictional forces did not extrapolate to zero at zero applied load thus indicating an adhesional component to the normal force.

The adhesional pull off forces are listed in Table XIII for the polymer coated fibers.

Table XIII

Adhesional Pull-Off Forces for the Polymer Films

Film	Pull-off Force (μN)
polystyrene	5.0 ± 0.3
polycarbonate	2.2 ± 0.2
polyethylene terephthalate	2.3 ± 0.2



ORIGINAL PAGE IS
OF POOR QUALITY

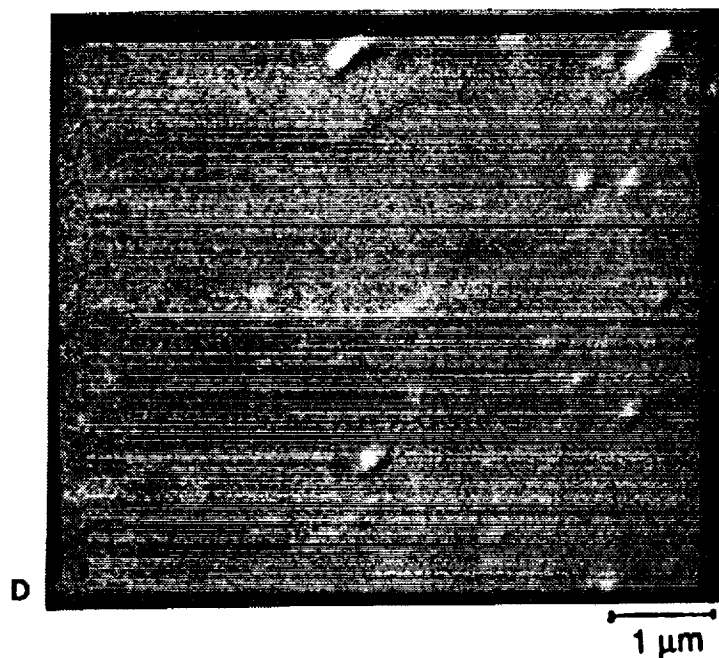
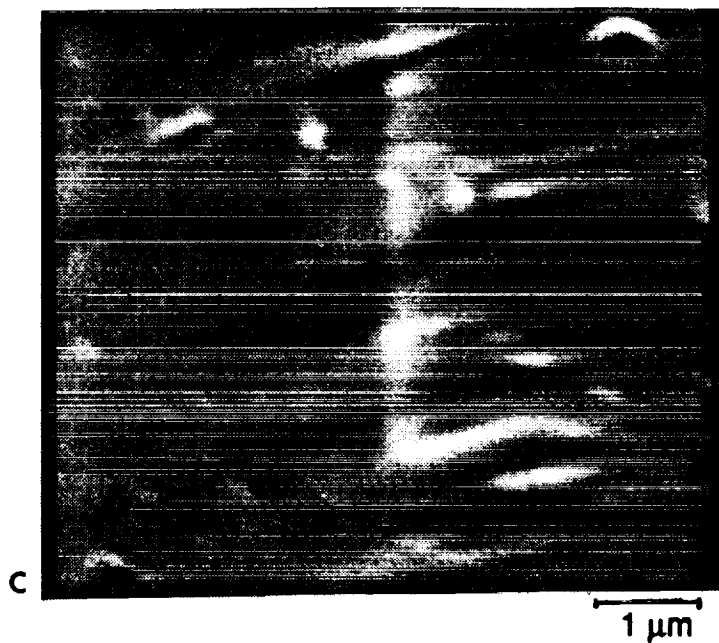


Figure 32 - Scanning electron micrographs of (A) the cross section and (B) the surface of PC deposited on silica fiber and the surfaces of (C) PS and (D) PET on silica fibers.

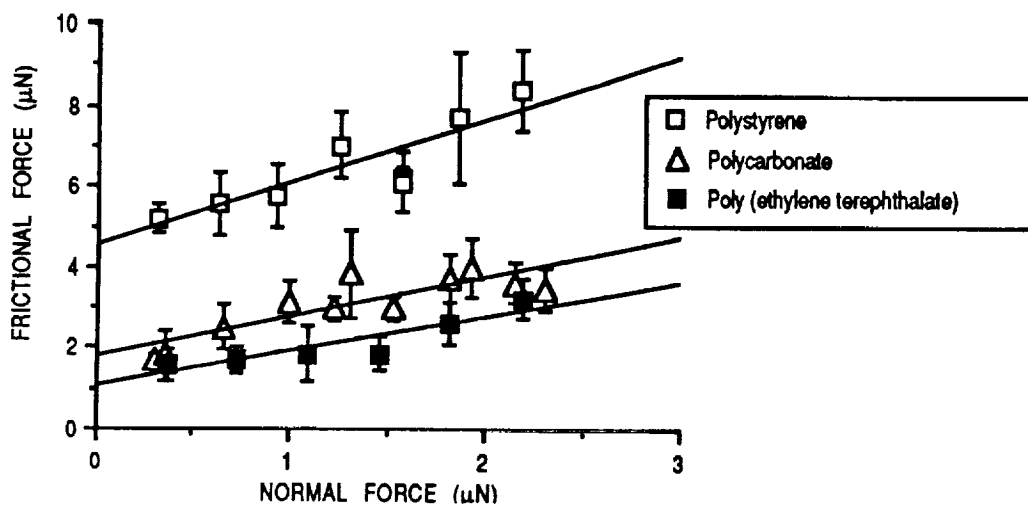


Figure 33 - Frictional behavior of polymer films of PS, PC and PET on silica fibers measured in air.

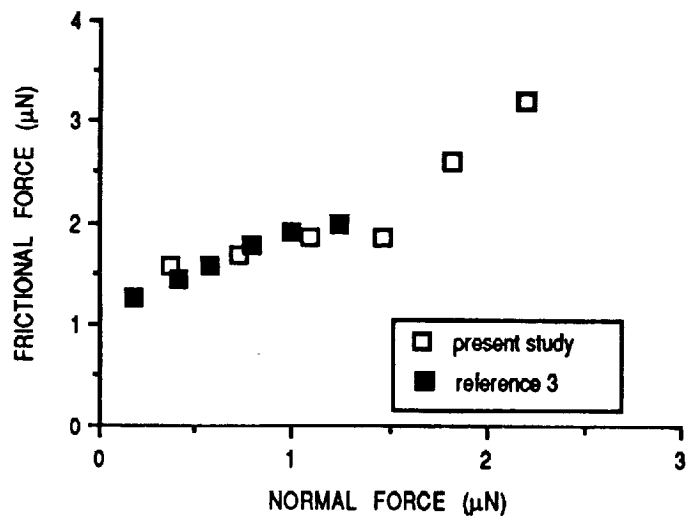


Figure 34 - Comparison of the frictional behavior of the PET film in the present study with that reported for PET fibers by Adam et al. (3)

The pull-off forces for PC and PET were about equal, whereas the pull-off force for PS was twice that of the other films. In all cases, the pull-off forces were observed to be independent of the rates of separation which indicates that viscoelastic effects were not appreciable. Note the good correspondence between the pull-off forces and the frictional forces at zero applied load obtained from the extrapolation of the regression lines in Figure 33. Evidently, the deformation micro-mechanisms are similar in the rupture of contact junctions for the adhesional (pull-off) experiments and the friction tests. This correspondence was not the case for freshly drawn silica fibers or for silica fibers with thin, adsorbed monolayers.

Assuming that contact deformation is wholly elastic, the area of contact can be calculated from the Hertzian analysis of contact including the 'pull-off' adhesional force (F_c). Table XIV summarizes the bulk mechanical parameters (45) used for the calculation of the area of contact.

Figure 35 shows the shear strength versus the applied pressure and it is evident that τ is a linear and increasing function of P that can be expressed by,

$$\tau = \tau_0 + \alpha P \quad [32]$$

where τ_0 is the shear strength at zero applied load and α is a constant. This linear relationship has been observed for other polymer systems as well as adsorbed monolayers (42, 46, 47). Table XV compares the values of τ_0 for PS, PC, and PET determined in the present study, by others using friction tests (48, 49) and the bulk shear strengths (48). The low value of the shear strength in the thin polymer films as compared with the bulk material is probably due to the high degree of orientation induced in the film by the sliding process itself. Briscoe and Tabor (50) observed that for polymers which are not readily oriented, the discrepancy between the thin film shear strength and the bulk shear strength is small.

TABLE XIV
Mechanical Data^a used in the
Calculation of the Contact Area
for the Polymer Coatings

	E (GPa)	Poisson's Ratio
PS	3.2	0.45
PC	2.35	0.40
PET	4.3	0.40

^a reference (53)

TABLE XV
Values of τ_0 for the Polymer Coatings

Polymer film	τ_0 (MPa)	τ_0 (MPa)	τ (Bulk)
PS	12.1	4.0 ^a	80.2 ^a
PC	6.3	-	-
PET	3.5	(4-5) ^a	29.4 ^a

^a reference (58)

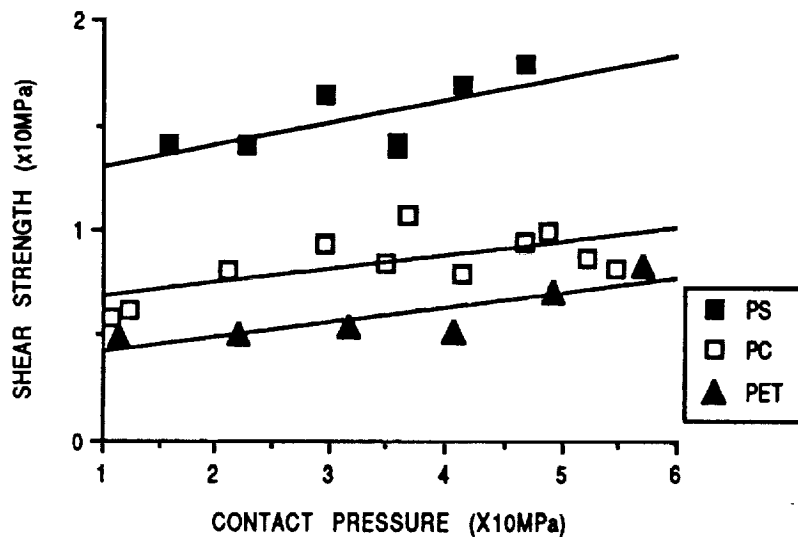
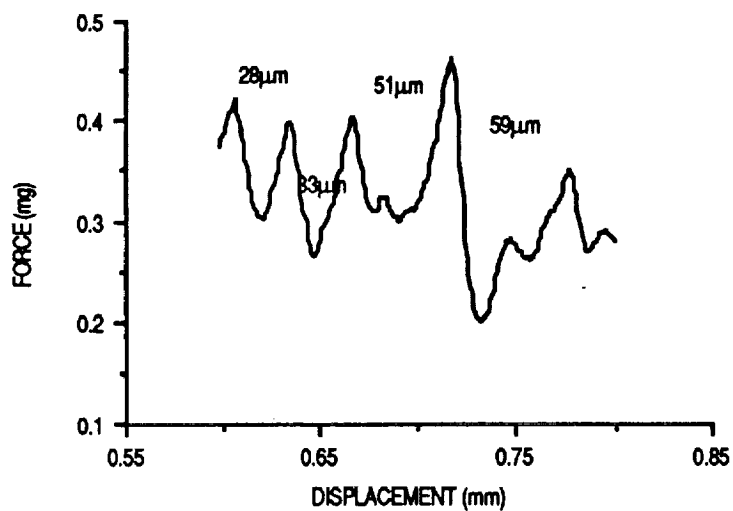
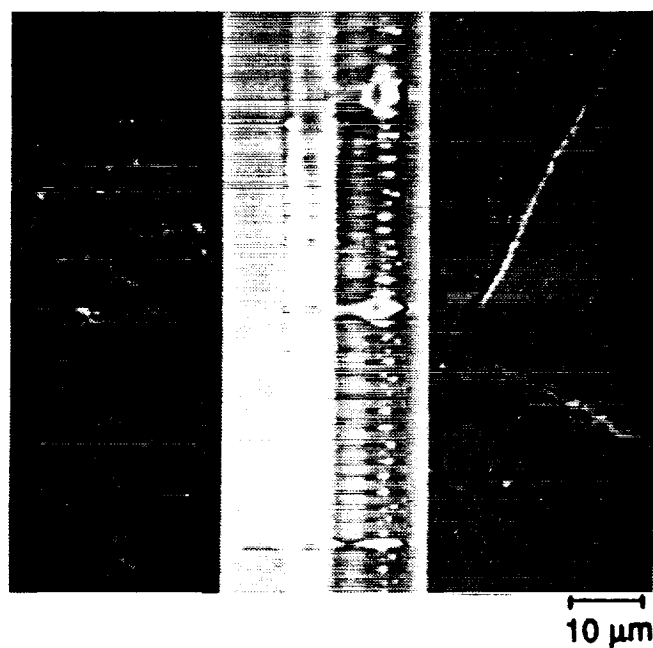


Figure 35 - Pressure dependence of the shear strength of PS, PC and PET films

In the experiments in PART I and PART II, efforts were made to observe wear tracks on the fiber surfaces using scanning electron microscopy. These efforts were unsuccessful probably because of the small area of contact. However, in the case of the polymer films, wear tracks were observable due to their lower yield strength compared to the uncoated and monolayer coated fibers.

Figure 36A shows a scanning electron micrograph of a PC coated silica fiber after friction measurements at a relatively high load ($2.5 \mu\text{N}$). A series of discrete traction marks are evident. The distances between peaks ranged between $30 - 60 \mu\text{m}$ (Figure 36B) which corresponds to the distances between the major traction marks observed using SEM. The area of the large torn circle was of the order of 10^{-12} m^2 while the calculated real area of contact was smaller by a factor of 10. This difference is probably the result of micro-deformation occurring as the junction is broken.

ORIGINAL PAGE
BLACK AND WHITE PHOTOGRAPH



ORIGINAL PAGE IS
OF POOR QUALITY

Figure 36 (A) Scanning electron micrograph of a PC film after friction measurement; (B) friction trace of the polycarbonate film. Numbers in μm represent the distance between peaks.

CONCLUSIONS

Results are reported on the friction and adhesion of polystyrene (PS), polycarbonate (PC) and polyethylene terephthalate (PET) coated silica fibers. The polymer films had relatively rough surfaces when they were examined using scanning electron microscopy. However, single point contact was assumed since the surface asperities were widely spaced and the area of contact being much smaller than this spacing. Interfacial shear strengths were calculated and the agreement was reasonably good when compared to published data from other friction measurements. The interfacial shear strengths were a factor of 7 to 10 less than the isotropic bulk shear strengths of the polymers. This difference is attributed to reorientation of the molecular structure in the interfacial layers as well as to the existence of well defined shear plane during sliding.

At higher applied loads, a series of discrete traction tears were produced. The pattern of the torn regions appeared as a series of transverse bands. One possible explanation for these bands is "microslip" of the fibers as the junction is failing resulting in greater local damage than occurs during the failure of junctions between uncoated silica fibers and silica fibers with adsorbed films. Briscoe (51) observed microslip for PET fibers which he defines as " --very slow relative movement that occurs at the apparent stick points."

PART IV FRICTIONAL BEHAVIOR OF TPS FIBERS

BACKGROUND

Fibers supplied by the Thermal Protection Materials Branch, NASA Ames Research Center were tested for their frictional behavior using the methods described in the preceeding sections. The fibers were tested as received and after heat treatment. An effort was made to use the information generated in the study of flame drawn silica fibers to interpret the results with the TPS fibers.

EXPERIMENTAL

The fibers obtained from Ames are listed in Table XVI along with known information on sizing. The fibers were tested as received and after heat treatment at 500°C for 4hrs.

Table XVI
Fibers obtained from NASA Ames Research Center

Fiber	Sizing
silicon carbide ^a	yes ^e
aluminoborosilicate ^b	yes ^e
silica ^c	aminopropylsilane ^d
boron nitride coated silicon carbide	no

^aNicalon NLM-102

^bNextel 312

^cAstroquartz, J. P. Stevens & Co.

^dA-1100, Union Carbide

^e proprietary coating, composition unknown

RESULTS

The frictional results for the fibers listed in Table XVI are presented in Figs. 37-40. The data were analyzed in terms of Eq. 29 to obtain values for M and the exponent n which for single asperite contact should be in the range of 0.65-0.75 (ideally $n = 0.67$). The constant M reflects the fiber diameter and modulus (Eq. 28). In addition the intercept of the data at $N = 0$ is taken as a measure of

the adhesional force, F_a , for each fiber type. These parameters are given in Table XVII.

Table XVII

Parameters Derived from TPS Fiber Frictional Behavior

fiber	M	n	τ_0 MPa	α	F_a μN
silica as received	0.224	0.64	72	0.97	0.5
heat cleaned	a	a	a	a	1.3
aluminoboro- silicate as received	0.441	0.20	a	a	2.1
heat cleaned	0.445	0.75	196	1.83	0.6
silicon carbide as received	0.929	0.67	82	a	2.3
heat cleaned	0.592	0.28	a	0.095	2.7
silicon carbide- boron nitride coated as received	0.292	0.61	91	1.21	0.6
heat cleaned	0.859	0.84	ND	ND	1.1

a data scatter too great to derive meaningful parameters

ND not determined

The following fibers gave values close to the range of $n = 0.65-0.75$;

silica- as received (0.64)

aluminoborosilicate - heat cleaned (0.75)

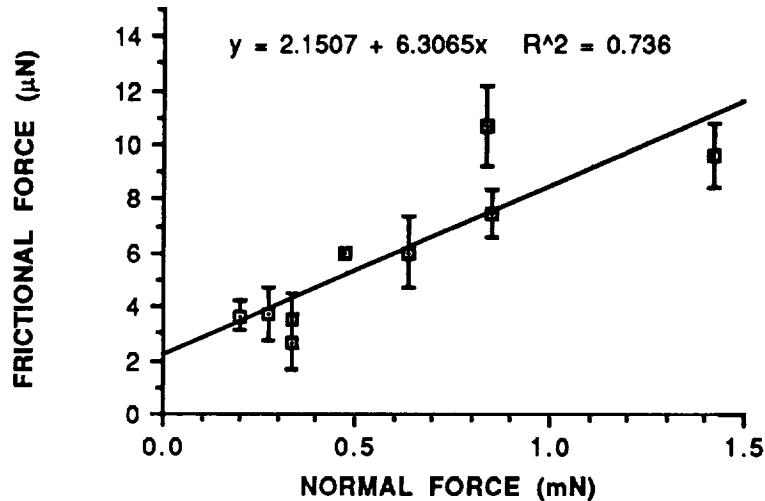
silicon carbide-as received (0.67)

boron nitride coated silicon carbide-as received (0.61)

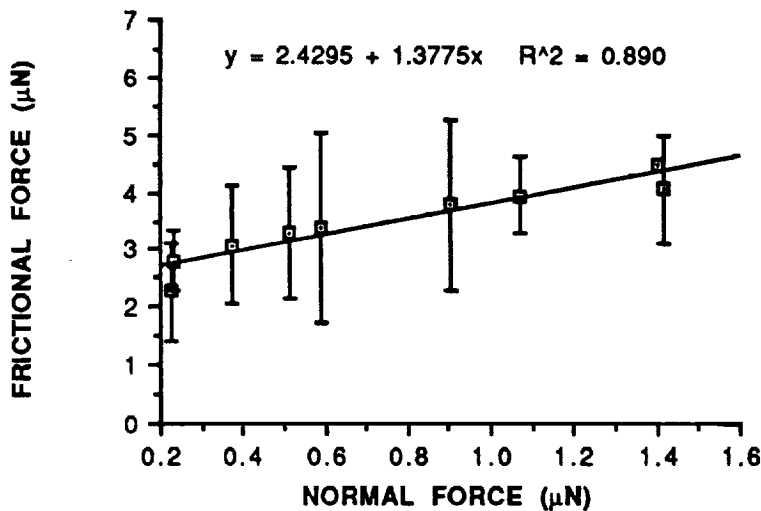
Presumably these fibers are sufficiently smooth to allow single point contact. Those fibers for which $n \neq 0.65 - 0.75$ are presumably rough resulting in multi-asperite contact, for which $n \rightarrow 1$. This was clearly the case for the BN-coated silicon carbide fiber

after heat treatment as evidenced from SEM photomicrographs showing surface cracks on the heat treated fiber (52).

However, the other fibers for which $n \neq 0.65 - 0.75$ gave exponents in the range of 0.2 - 0.3 (as received aluminoborosilicate and heat treated silicon carbide). The physical significance of these low n values is not immediately obvious.

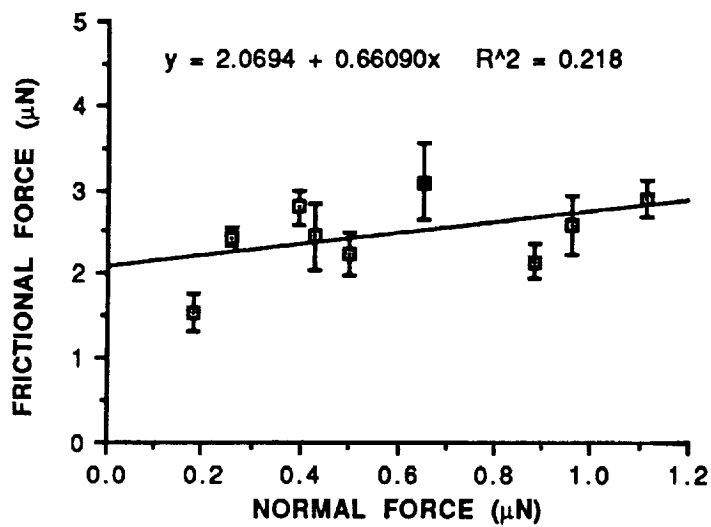


A

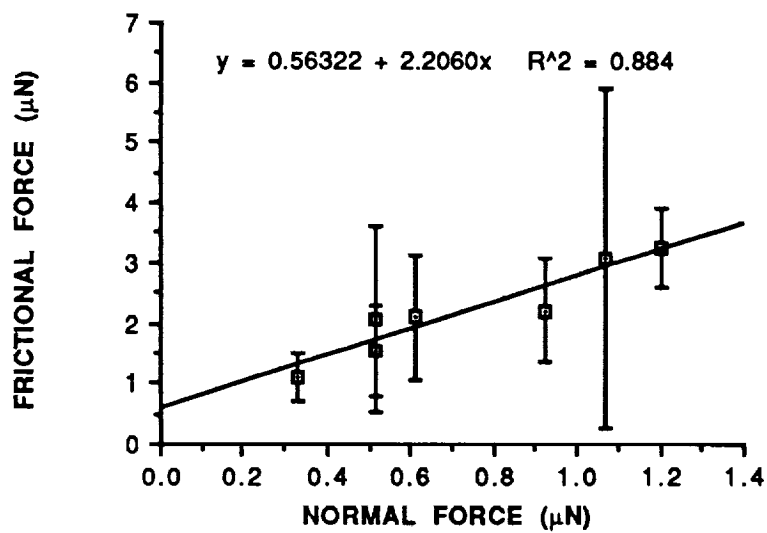


B

Figure 37 - Frictional force vs normal force for silicon carbide fibers as received (A) and after heat treatment (B).

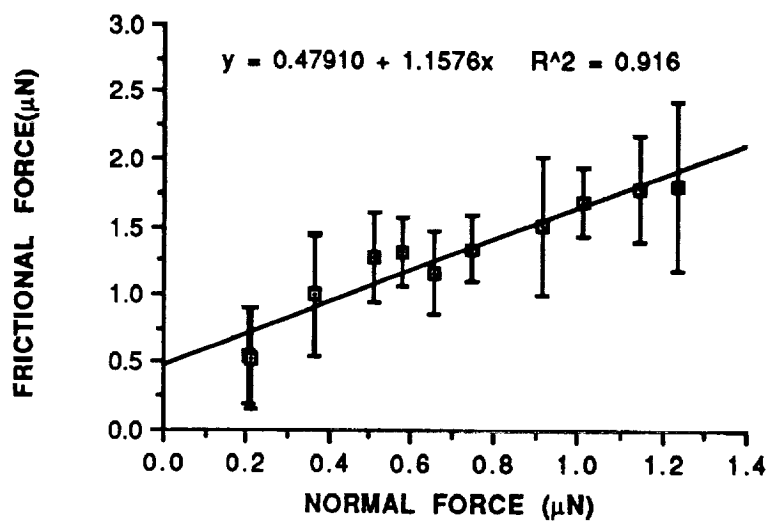


A

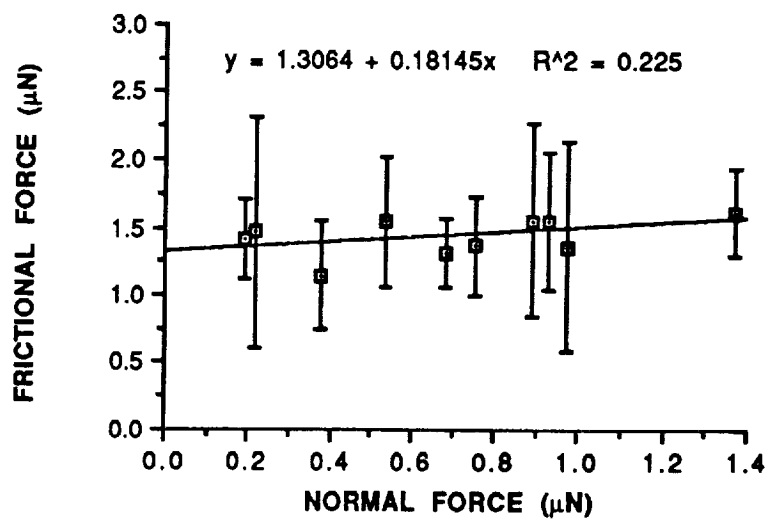


B

Figure 38 - Frictional force vs normal force for aluminoborosilicate fibers as received (A) and after heat treatment (B)

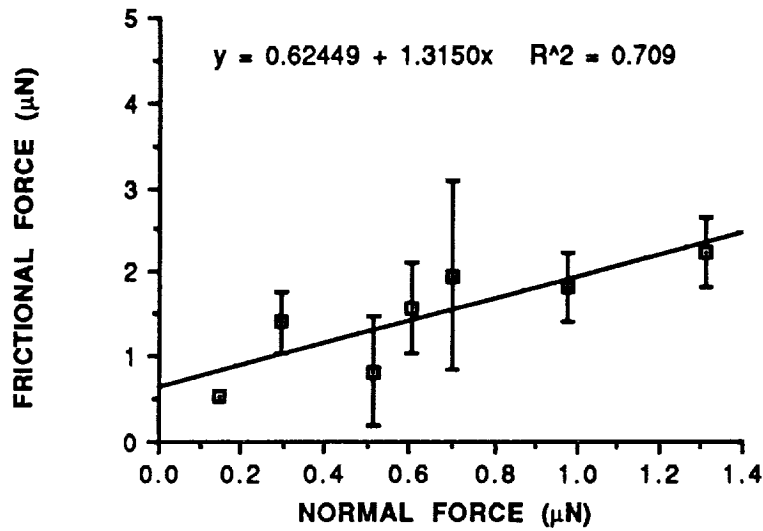


A

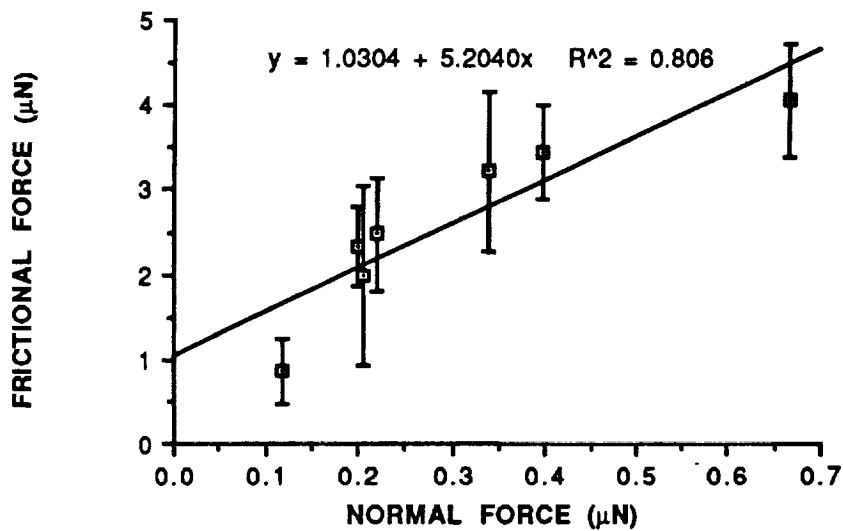


B

Figure 39 - Frictional force vs normal force for silica fibers as received (A) and after heat treatment (B).



A



B

Figure 40 - Frictional force vs normal force for boron nitride coated silicon carbide fibers as received (A) and after heat treatment (B)

The friction data were recalculated in terms of contact shear strength vs contact pressure in order to obtain the parameters, τ_0 and α (Eq. 32). These calculations require measurement of the

adhesional pull off forces which are listed in Table XVIII. Plots of shear strength vs contact pressure are presented in Figs. 41 - 44.

Table XVIII

Adhesional Pull-Off Forces for the TPS Fibers

Fiber	Condition	Diameter (μm)	E(GPa)	Pull-Off Force(μN)
silica	as received	9.3	75	0.98
	heat treated			0.2
silicon carbide	as received	15	196	17.5
	heat treated			3.23
alumino-borosilicate	as received	11.8	176	1.57
	heat treated			0.2
boron nitride coated silicon carbide	as received	15	0.25	2.55

Poisson's Ratio = 0.24 for all cases.

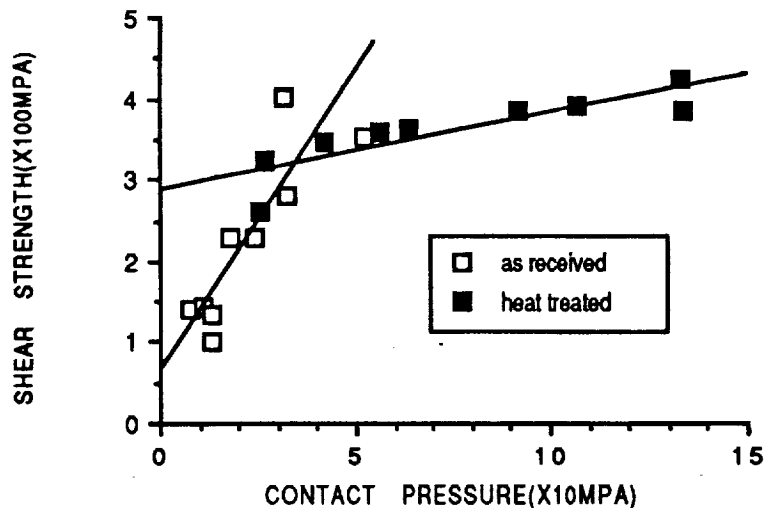


Figure 41 - Shear strength vs contact pressure for silicon carbide fibers.

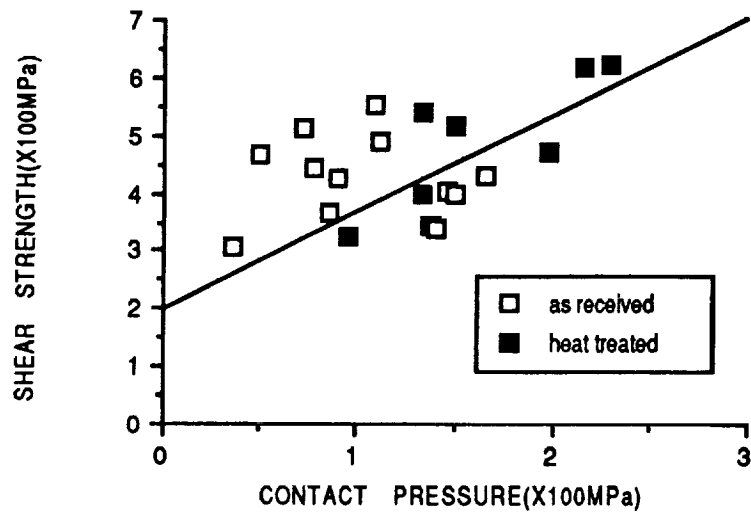


Figure 42 - Shear strength vs contact pressure for aluminoborosilicate fibers.

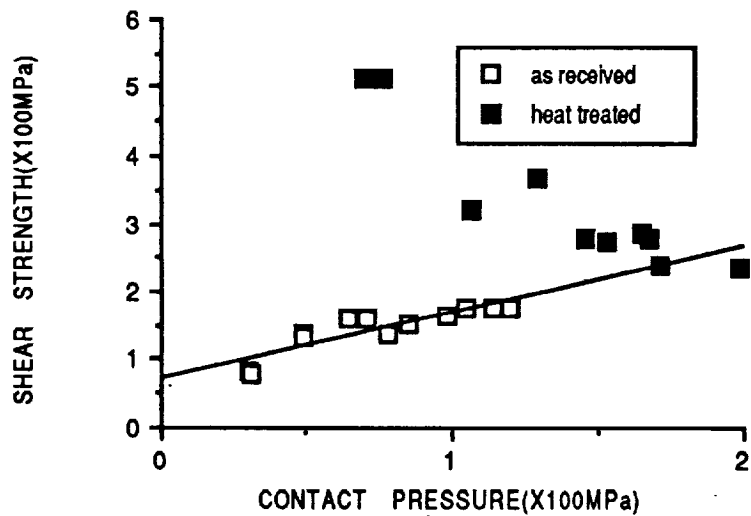


Figure 43 - Shear strength vs contact pressure for silica fibers.

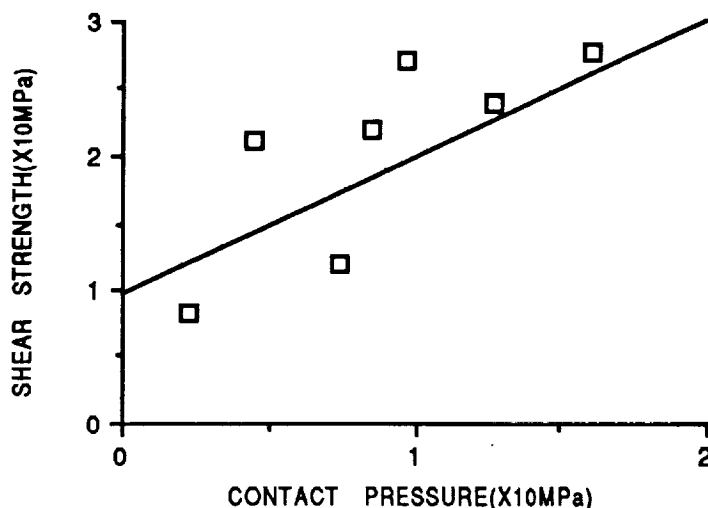


Figure 44 - Shear strength vs contact pressure for boron nitride coated silicon carbide fibers (as received).

CONCLUSIONS

The TPS fibers all exhibited slip-stick sliding friction as expected. Only four of the fibers met the criteria for single asperite contact. Note that these same fibers gave reasonably linear plots of shear strength vs contact pressure from which values of τ_0 and α could be obtained. As was the case for flame drawn silica, the shear strengths, τ_0 , are much lower than would be expected for the corresponding bulk materials.

The adhesional pull-off forces (Table XVIII) were generally larger than the adhesion force, F_a , estimated from the friction data at zero applied load (Table XVII). This difference has been the case for uncoated flame drawn silica and for silica fibers with adsorbed monolayers. However, in the tests of silica with thick polymer films the pull-off forces and the F_a values were comparable. One might have expected that the TPS fibers with a sizing coating would behave similar to the polymer coated silica fibers. This not being the case suggests that the sizing coatings are thin so that the deformations that occur during pull-off are dominated by tensile forces whereas in the friction test the rupture of contact junctions is dominated by shearing forces.

REFERENCES

1. B. J. Briscoe and S. L. Kremnitzer, "A Study of the Friction and Adhesion of Polyethylene Terephthalate Monofilaments," J. Phys. D. Appl., 12, 505 (1979)
2. M. J. Adams, B. J. Briscoe and S. L. Kremnitzer, "The Effect of Liquids on the Autoadhesion and Friction of Polyethylene Terephthalate Monofilaments," in Microscopic Aspects of Adhesion and Lubrication, J. M. George, Ed., Elsevier, Amsterdam, 1982, p. 405
3. M. J. Adam, B. J. Briscoe and S. L. Kremnitzer, "A Survey of Adhesion, Friction and Lubrication of Poly Ethylene Terephthalate Monofilaments," in Physicochemical Aspects of Polymer Surfaces, K. L. Mittal, Ed., Plenum Press, New York, 1983a, p.425
4. M. J. Adams, E. O'Keefe, B. J. Briscoe and S. L. Kremnitzer, J. Phys. D: Appl.Phys 16, L9 (1983b)
5. B. J. Briscoe, T. K. Wee, A. Winkler, and M. J. Adams, "Wear of Poly(ethylene terephthalate) Monofilaments in Polymer Wear and its Control", ACS Symposium Series 287, 375 (1985)
6. Roselman, I. C. and Tabor, D., "The Friction of Carbon Fibres," J. Phys. D: Appl. Phys. 9 2517 (1976)
7. F. P. Bowden and D. Tabor, The Friction and Lubrication of Solids, Clarendon press, Oxford, Vol I 1950
8. F. P. Bowden and D. Tabor, The Friction and Lubrication of Solids, Clarendon Press, Oxford, Vol II 1964
9. A. R. Savkoor, "The Mechanics and Physics of Adhesion of Elastic Solids," in Microscopic Aspects of Adhesion and Lubrication, J. M. George, Ed., Elsevier, New York, 1982, p. 279
10. R. S. Bradley, "Adsorption at the Surface of Binary Liquid Mixtures," Phil. Mag., Z, 142 (1932)
11. B. V. Derjaguin, V. M. Muller, and Yu. P. Toporov, "Effect of Contact Deformations on the Adhesion of Particles," J. Colloid Interface Sci., 53 314 (1975)

12. B. V. Derjaguin, V. M. Muller, and Yu. P. Toporov, "Effect of Contact Deformations on the Adhesion of Particles," J. Colloid and Interface Sci. 67, 378 (1978)
13. B. V. Derjaguin, V. M. Muller, and Yu. P. Toporov, "Effect of Contact Deformations on the Adhesion of Particles," Colloid Surf., 7, 251 (1983)
14. K. L. Johnson, K. Kendall, and A. D. Roberts, Surface Energy and the Contact of Elastic Solids, Proc. R. Soc. Lond. A. 324 301 (1971)
15. M. D. Pashley, J. B. Pethica and D. Tabor, "Adhesion and Micromechanical Properties of Metal Surfaces," Wear, 100 7 (1984)
16. D. Dowson, History of Tribology, Longman, London, 1979
17. G. A. Tomlinson, Phil. Mag., 34 143 (1929)
18. J. F. Archard, "Elastic Deformation and the Laws of Friction," Proc. Roy. Soc. London A243 190 (1957)
19. D. Tabor, "Friction-The Present State of Our Understanding," Trans. J. Lub. Tech. 103 169 (1981)
20. M. J. Shick, Surface Characteristics of Fibers and Textiles, Marcel Dekker, NY, 1977, p. 417
21. R. L. Scheaffer and J. T. McClave, Probability and Statistics for Engineers, 2nd Edition, Duxbury Press, Boston, 1986, p. 152
22. R. K. Iller, Colloid Chemistry of Silica and Silicates, Cornell University Press, Ithaca, NY., 1955, p.622
23. J. N. Israelachvili and D. Tabor, "The Measurement of van der Waals Dispersion Forces in the Range 1.5 to 130 nm," Proc. Roy. Soc., London, A331, 19 (1972)
24. A. Kohno and S. Hyodo, "The Effect of Surface Energy on the Microadhesion between Hard Solids," J. Phys. D: Phys., 7 1243 (1974)
25. J. N. Israelachvili, Intermolecular and Surface Forces, Academic Press, New York, 1985

26. A. W. Newman, S. N. Omenyi and C. J. van Oss, *Colloid Polymer Sci.*, 257 413 (1979)
27. K. N. G. Fuller and D. Tabor, "The Effect of Surface Roughness on the Adhesion of Elastic Solids," *Proc. Roy. Soc. London*, A345, 3, 327 (1975)
28. K. L. Johnson, Contact Mechanics, Cambridge Univ. Press, Cambridge, 107-144 (1985)
29. S. Timoshenko and J. D. Goodier, Theory of Elasticity, 2nd Ed., McGraw Hill, NY, 1951
30. B. V. Derjaguin and Yu. P. Toporov, "Influence of Adhesion on Sliding and Rolling Friction," in, Microscopic Aspects of Adhesion and Lubrication, *Tribo. Series 7*, Elsevier, New York, 343-353, 1982
31. A. R. Savkoor and G. A. D. Briggs, "The Effect of Tangential Force on the Contact of Elastic Solids in Adhesion," *Proc. R. Soc. Lond. A* 356 103 (1977)
32. R. F. King and D. Tabor, "The Strength Properties and Frictional behavior of Brittle Solids," *Proc. Roy. Soc., London, Ser.*, A223, 221 (1954)
33. J. N. Israelachvili, L. R. Fisher, R. G. Horn and H. K. Christenson, "Measurement of Adhesion and Short-Range Forces Between Molecularly Smooth Surfaces in Undersaturated Vapors and in Organic Liquids," in Microscopic Aspects of Adhesion and Lubrication, J. M. Georges Ed., Elsevier, New York, 55 (1982)
34. E. Rabinowicz and D. Tabor, "Metallic Transfer between Sliding Metals: an Autoradiographic Study," *Proc. Roy. Soc., London*, A208, 455 (1951)
35. W. C. Bigelow, D. L. Pickett and W. A. Zisman, "Oleophobic Monolayers; I. Films Adsorbed from Solution in non-Polar Liquids," *J. Colloid Interface Sci.*, 1, 513 (1946)
36. J. M. Park and J. D. Andrade, "Dynamic Contact Angle Studies of n-Alkyl Derivatized Boro-Silicate Glass Surfaces," in Polymer

Surface Dynamics, J. D. Andrade ed., Plenum Press, New York, 1988, p. 67

37. A. Dorinson and K. C. Ludema, "Lubricant Additive Action," in Mechanics and Chemistry in Lubrication, Elsevier, New York, 1985, P.178

38. W. A. Zisman, "Relation of the Equilibrium Contact Angle to Liquid and Solid Constitution," in Contact Angle, Wettability, and Adhesion, American Chemical Soc., Washington, DC, Adv. Chem. Ser., 43, 1 (1964)

39. C. Bigelow and L. O. Brockway, "Variation of Contact Angle and Structure with Molecular Length and Surface Density in Adsorbed Films on Fatty Acids," J. Colloid Interface Sci., 11, 60 (1956)

40. W. D. Bascom, "The Wettability of n-Octadecylamine, n-Octadecyl Alcohol and n-Octadecanoic Acid Films Adsorbed on Thermally Treated Metal Oxide Surfaces," J. Colloid Interface. Sci., 26, 89 (1968)

41. O. Levine and W. A. Zisman, "Physical Properties of Monolayers Adsorbed at the Solid-Air Interface I: Friction and Wettability of Aliphatic Polar Compounds and Effect of Halogenation," J. Phys. Chem., 61, 1068 (1957)

42. B. J. Briscoe, B. Scruton and F. R. Willis, "The Shear Strength of Thin Lubricant Films," Proc. Roy. Soc., London, A333 99 (1973)

43. B. J. Briscoe and A. C. Smith, "Time Dependence Effects in the Shear of Thin Polymeric Films," J Phys. D: Appl. Phys. 15 579 (1982)

44. B. J. Briscoe, "Tribology of Polymers," in, Physicochemical Aspects of Polymer Surfaces, K. L. Mittal Ed., Plenum Press, NY, 1981, p. 387

45. I. M. Ward, Mechanical Properties of Solid Polymers, Wiley Interscience, London, 1971, p. 243

46. J. K. A. Amuzu, B. J. Briscoe and M. M. Chaudhri, "Frictional Properties of Explosives," J. Phys. D: Appl. Phys., 9 133 (1976)

47. L. C. Towle, "Shear Strength and Friction Measurements on Thin Layers under High Pressure," J. Appl. Phys., 42 2369 (1971)
48. B. J. Briscoe and D. Tabor, "Shear Properties of Thin Polymeric Films," J. Adhesion, 9 145 (1978)
49. B. J. Briscoe, "Interfacial Friction of Polymer Composites, General Fundamental Principles," in Friction and Wear of Polymer Composites, K Friedrich Ed., Elsevier, NY, 1986, p. 25
50. B. J. Briscoe and D. Tabor, The Effect of Pressure on the Frictional Properties of Polymers, Wear, 34 29 (1975)
51. B. J. Briscoe, A. Winkler and M. J. Adams, "A Statistical Analysis of the Frictional Forces Generated Between Monofilaments during Intermittent Sliding, " J. Phys. D: Appl. Phys., 18 2143 (1985)
52. Letter Report, D. A. Kourtides, Nov. 8, 1988